Adaptive Denoising via GainTuning

Sreyas Mohan[1], **Joshua L. Vincent**[2], **Ramon Manzorro**[2], **Peter A. Crozier** [2],
Carlos Fernandez-Granda[1,3], **Eero P. Simoncelli**[1,3,4]

[1]Center For Data Science, NYU,
[2]School for Engineering of Matter, Transport and Energy, ASU
[3]Courant Institute of Mathematical Sciences, NYU
[4]Center for Neural Science, NYU and Flatiron Institute, Simons Foundation

Abstract

Deep convolutional neural networks (CNNs) for image denoising are typically trained on large datasets. These models achieve the current state of the art, but they do not generalize well to data that deviate from the training distribution. Recent work has shown that it is possible to train denoisers on a single noisy image. These models adapt to the features of the test image, but their performance is limited by the small amount of information used to train them. Here we propose "GainTuning", a methodology by which CNN models pre-trained on large datasets can be adaptively and selectively adjusted for individual test images. To avoid overfitting, GainTuning optimizes a single multiplicative scaling parameter (the "Gain") of each channel in the convolutional layers of the CNN. We show that GainTuning improves state-of-the-art CNNs on standard image-denoising benchmarks, boosting their denoising performance on nearly every image in a held-out test set. These adaptive improvements are even more substantial for test images differing systematically from the training data, either in noise level or image type. We illustrate the potential of adaptive GainTuning in a scientific application to transmission-electron-microscope images, using a CNN that is pre-trained on synthetic data. In contrast to the existing methodology, GainTuning is able to faithfully reconstruct the structure of catalytic nanoparticles from these data at extremely low signal-to-noise ratios.

1 Introduction

Like many problems in image processing, the recovery of signals from noisy measurements has been revolutionized by the development of convolutional neural networks (CNNs) [66, 8, 67]. These models are typically trained on large databases of images, either in a supervised [37, 66, 8, 68, 67] or an unsupervised fashion [62, 3, 27, 29]. Once trained, these solutions are evaluated on noisy test images. This approach achieves state-of-the-art performance when the test images and the training data belong to the same distribution. However, when this is not the case, the performance of these models is often substantially degraded [59, 37, 68]. This is an important limitation for many practical applications, in which it is challenging (or even impossible) to gather a training dataset that is comparable in noise and signal content to the images encountered at test time. Overcoming this limitation requires *adaptation* to the test data.

A recent unsupervised method (Self2Self) has shown that CNNs can be trained exclusively on individual test images, producing impressive results [46]. Despite this, the performance of Self2Self is limited by the small amount of available training information, and is generally inferior to CNN models trained on large databases.
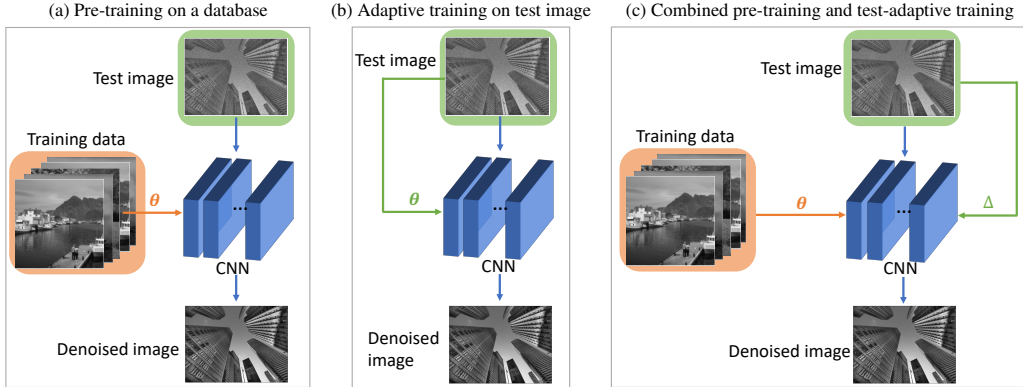
Figure 1: **Proposed denoising paradigm**. (a) Typically, CNNs are trained on a large dataset and evaluated directly on a test image. (b) Recent unsupervised methods perform training on a single test image. (c) We propose GainTuning, a framework which bridges the gap between both of these paradigms: a CNN pre-trained on a large training database is adapted to the test image.

In this work, we propose *GainTuning*, a framework to bridge the gap between models pre-trained on large datasets, and models trained exclusively on test images. In the spirit of two recent methods [55, 59], GainTuning adapts pre-trained CNN models to individual test images by minimizing an unsupervised denoising cost function, thus fusing the generic capabilities obtained from the training data with specific refinements matched to the structure of the test data. Rather than adapt the full parameter set (filter weights and additive constants) to the test image, GainTuning instead optimizes a single multiplicative scaling parameter (the "Gain") for each channel within each layer of the CNN. The dimensionality of this reduced parameter set is a small fraction ($\approx 0.1\%$ in our examples) of that of the full parameter set. We demonstrate through extensive examples that this prevents overfitting to the test data. The GainTuning procedure is general, and can be applied to any CNN denoising model, regardless of the architecture or pre-training process.

Our contributions. GainTuning provides a novel method for adapting CNN denoisers trained on large datasets to a single test image. GainTuning improves state-of-the-art CNNs on standard image-denoising benchmarks, boosting their denoising performance on nearly every image in held-out test sets. Performance improvements are even more substantial when the test images differ systematically from the training data. We showcase this ability through controlled experiments in which we vary the distribution of the noise and image structure of the test data. Finally, we evaluate GainTuning in a real scientific-imaging application where adaptivity is crucial: denoising transmission-electron-microscope data at extremely low signal-to-noise ratios. As shown in Figure 2, both CNNs pre-trained on simulated images and CNNs trained only on the test data produce denoised images with substantial artefacts. In contrast, GainTuning achieves effective denoising, accurately revealing the atomic structure in the real data.

2   Related Work

Denoising via deep learning. In the last five years, CNN-based methods have clearly outperformed previous state-of-the-art denoising methods [13, 53, 6, 45, 14, 21, 10]. Denoising CNNs are typically trained in a supervised fashion, minimizing mean squared error (MSE) over a large database of example ground-truth clean images and their noisy counterparts [66, 37, 8]. Unsupervised methods have also been developed, which do not rely on ground-truth images. There are two main strategies to achieve this: use of an empirical Bayes objective, such as Stein's unbiased risk estimator (SURE) [13, 33, 48, 36, 55, 56], and architectural "blind-spot" methods [27, 29, 3, 62] (see Section 4 for a more detailed description).

Generalization to out-of-distribution noise. Previous studies have shown that CNN denoisers fail to generalize when the noise encountered at test time differs from that of the training data [68, 37]. Ref. [37] proposes the use of a modified CNN architecture without additive bias terms, which is able to generalize to noise with variance well beyond that encountered in the training set. Here, we show
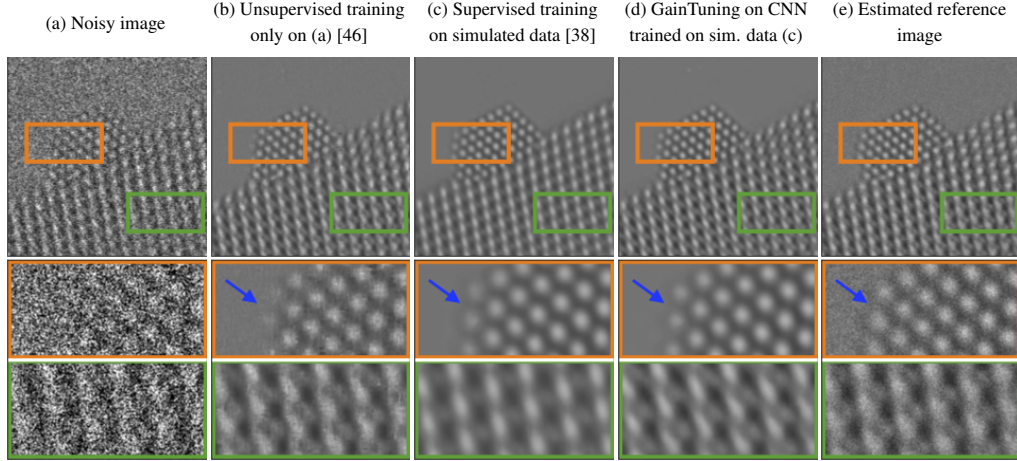
Figure 2: **Denoising results for real-world data.** (a) An experimentally-acquired atomic-resolution transmission electron microscope image of a CeO2-supported Pt nanoparticle. The image has a very low signal to noise ratio (PSNR of $\approx 3dB$). (b) Denoised image obtained using Self2Self [46], which fails to reconstruct three atoms (blue arrow, second row). (c) Denoised image obtained via a CNN trained on a simulated dataset, where the pattern of the supporting atoms is not recovered faithfully (third row). (d) Denoised image obtained by adapting the CNN in (c) to the noisy test image in (a) using GainTuning. Both the nanoparticle and the support are recovered without artefacts. (e) Reference image, estimated by averaging 40 different noisy images of the same nanoparticle.

that augmenting a generic architecture with GainTuning yields comparable performance to removing bias.

Generalization to out-of-distribution images. In order to adapt CNNs to operate on test data with characteristics differing from the training set, recent publications propose fine-tuning the networks using an additional training dataset that is more aligned with the test data [59, 18]. This is a form of transfer learning, a popular technique in classification problems [12, 64]. However, it is often challenging to obtain relevant additional training data. Here, we show that GainTuning can adapt CNN denoisers to novel test images.

Feature normalization. Normalization techniques such as batch normalization (BN) [23] are a standard component of deep CNNs. BN consists of two stages: (1) centering and normalizing the features corresponding to each channel, (2) scaling and shifting the normalized features using two learned parameters per channel (a scaling factor and a shift). The scaling parameter is analogous to the gain parameter introduced in GainTuning. However, in BN this parameter is adjusted during training and fixed during test time, whereas GainTuning adjusts it adaptively, for each test image.

Gain normalization. Motivated by gain control properties observed in biological sensory neurons [5], adaptive local normalization of response gains has been previously applied in object recognition [24], density estimation [1], and compression [2]. In contrast to these approaches, which adjust gains based on local responses, GainTuning adjusts a global gain for each channel by optimizing an unsupervised objective function.

Adapting CNN denoisers to test data. Two recent publications have developed methods of adapting CNN denoisers to test data [56, 59]. Ref. [56] include the noisy test images in the training set. In a recent extension, the authors fine-tune a pre-trained CNN on a single test image using the SURE cost function [55]. Ref. [59] does the same using a novel cost function based on noise resampling (see Section 4 for a detailed description). As shown in Section E fine-tuning the full set of CNN parameters using only a single test image can lead to overfitting. Ref. [55] avoids this using early stopping, selecting the number of fine-tuning steps beforehand. Ref. [59] uses a specialized architecture with a reduced number of parameters. Here, we show that several unsupervised cost functions can be used to perform adaptation without overfitting, as long as we only optimize a subset of the model parameters (specifically, the gain of each channel).

Adjustment of channel parameters to improve generalization in other tasks. Adjustment of channel parameters, such as gains and biases, has been shown to improve generalization in multiple machine-learning tasks, such as the vision-language problems [43, 11], image generation [7], style transfer [17], and image restoration [20]. In these methods, the adjustment is carried out while training the model by minimizing a supervised cost function. In image classification, recent studies have proposed performing adaptive normalization [25, 41, 51] and optimization [61] of channel parameters during test time, in the same spirit as GainTuning.

3 Proposed Methodology: GainTuning

In this section we describe the GainTuning framework. Let f_θ be a CNN denoiser parameterized by weight and bias parameters, θ. We assume that we have available a training database and a test image $\mathbf{y}_\text{test}$ that we aim to denoise. First, the networks parameters are optimized on the training database

$$\theta_\text{pre-trained} = \arg\min_\theta \sum_{y \in \text{training database}} \mathcal{L}_\text{pre-training}(y, f_\theta(y)). \tag{1}$$

The cost function $\mathcal{L}_\text{pre-training}$ used for pre-training can be supervised, if the database contains clean and noisy examples, or unsupervised, if it only contains noisy data.

A direct method of adapting the pre-trained CNN to the test data is to finetune all the parameters, as is done in all prior work on test-time adaptation [59, 55, 18]. Unfortunately this can lead to *overfitting* the test data (see Section E). Due to the large number of degrees of freedom, the model is able to minimize the unsupervised cost function without denoising the noisy test data effectively. This can be avoided to some extent by employing CNN architectures with a small number of parameters [59], or by only optimizing for a short time ("early stopping") [55]. Unfortunately, using a CNN with reduced parameters can limit performance (see Section 5), and it is unclear how to choose a single criterion for early stopping that can operate correctly for all test images. Here, we propose a different strategy: tuning a single parameter (the *gain*) in each channel of the CNN. GainTuning can be applied to any pre-trained CNN.

We denote the gain parameter of the cth channel of the the lth layer as $\gamma[l, c]$, and the conventional parameters of that channel by $\theta_\text{pre-trained}[l, c]$ (a vector containing the filter weights). The adapted GainTuning parameters are the product of these:

$$\theta_\text{GainTuning}(\gamma)[l, c] = \gamma[l, c] \, \theta_\text{pre-trained}[l, c]. \tag{2}$$

We estimate the gains by minimizing an unsupervised loss that only depends on the noisy image:

$$\hat{\gamma} = \arg\min_\gamma \quad \mathcal{L}_\text{GainTuning}(\mathbf{y}_\text{test}, \theta_\text{GainTuning}(\gamma)) \tag{3}$$

The final denoised image is $f_{\theta_\text{GainTuning}(\hat{\gamma})}(\mathbf{y}_\text{test})$. Section 4 describes several possible choices for the cost function $\mathcal{L}_\text{GainTuning}$. Since we use only one scalar parameter per channel, the adjustment performed by GainTuning is very low-dimensional ($\approx 0.1\%$ of the dimensionality of θ). This makes optimization quite efficient, and prevents overfitting (see Section E). Further, in Section E we show that performing GainTuning provides better performance when compared to fine-tuning only the last few layers of the pre-trained network.

4 Cost Functions for GainTuning

A critical element of GainTuning is the use of an unsupervised cost function, which is minimized in order to adapt the pre-trained CNN to the test data. Here, we describe three different choices, each of which are effective for the GainTuning framework, but which have different benefits and limitations.

Blind-spot loss. This loss measures the ability of the denoiser to reproduce the noisy observation, while excluding the identity solution. To achieve this, the CNN must estimate the jth pixel y_j of the noisy image y as a function of the other pixels $y_{\{j\}^c}$, *excluding the pixel itself*. As long as the noise degrades pixels *independently*, the network to learn a nontrivial denoising function that exploits the relationships between pixels arising from the underlying clean image(s). The resulting loss can be written as

$$\mathcal{L}_\text{blind-spot}(\mathbf{y}, \theta) = \mathbb{E}\left[(f_\theta(\mathbf{y}_{\{j\}^c})_j - \mathbf{y}_j)^2\right]. \tag{4}$$

Here the expectation is over the data distribution and the selected pixel. This "blind spot" can be enforced through architecture design [29], or by masking [3, 27] (see also [46] and [62] for related approaches). The blind-spot loss has a key property that makes it very powerful in practical applications: it makes no assumption about the noise distribution beyond pixel-wise independence. When combined with GainTuning it achieves effective denoising of real electron-microscope data at very low SNRs (see Figure 2 and Section 5.4, F.5).

Stein's Unbiased Risk Estimator (SURE). Let $\mathbf{x}$ be an N-dimensional ground-truth random vector $\mathbf{x}$ and let $\mathbf{y} := \mathbf{x} + \mathbf{n}$ be a corresponding noisy observation, where $\mathbf{n} \sim \mathcal{N}(0, \sigma_n^2 \mathbf{I})$. SURE provides an expression for the MSE between $\mathbf{x}$ and a denoised estimate $f_\theta(\mathbf{y})$, which *only depends on the noisy observation* $\mathbf{y}$:

$$\mathbb{E}\left[\frac{1}{N}\|\mathbf{x} - f_\theta(\mathbf{y})\|^2\right] = \mathbb{E}\left[\frac{1}{N}\|\mathbf{y} - f_\theta(\mathbf{y})\|^2 - \sigma^2 + \frac{2\sigma^2}{N}\sum_{k=1}^{N}\frac{\partial(f_\theta(\mathbf{y})_k)}{\partial \mathbf{y}_k}\right] := \mathcal{L}_{\text{SURE}}(\mathbf{y}, \theta). \quad (5)$$

The last term in Equation 8 is the divergence of f_θ, which can be approximated using Monte Carlo techniques [47] (Section D). The divergence is the sum of the partial derivatives of each denoised pixel with respect to the corresponding input pixel. Intuitively, penalizing it forces the denoiser to not rely as heavily on the jth noisy pixel to estimate the jth clean pixel. This is similar to the blind-spot strategy, with the added benefit that the jth noisy pixel is not ignored completely. To further illustrate this connection, consider a linear convolutional denoising function $f_\theta(\mathbf{y}) = \theta \circledast \mathbf{y}$, where the center-indexed parameter vector is $\theta = [\theta_{-k}, \theta_{-k+1}, \ldots, \theta_0, \ldots, \theta_{k-1}, \theta_k]$. The SURE cost function (Equation 8) reduces to

$$\mathbb{E}_{\mathbf{n}}\left[\frac{1}{N}\|\mathbf{y} - \theta \circledast \mathbf{y}\|^2\right] - \sigma^2 + 2\sigma^2\theta_0 \quad (6)$$

The SURE loss equals the MSE between the denoised output and the noisy image, with a penalty on the "self" pixel. As this penalty is increased, the self pixel will be ignored, so the loss tends towards the blind-spot cost function. When integrated into the GainTuning framework, the SURE loss is limited to additive Gaussian noise, for which it outperforms the blind-spot loss. Extensions of SURE to many other stochastic observation models have been developed [49], and may offer alternative objectives for GainTuning.

Noise Resampling. Ref. [59] introduced a novel procedure for adaptation which we call *noise resampling*. Given a pre-trained denoiser f_θ and a test image $\mathbf{y}$, first one obtains an initial denoised image by applying f_θ to $\mathbf{y}$, $\hat{\mathbf{x}} := f_{\theta_{\text{pre-trained}}}(\mathbf{y})$. This denoised image is then artificially corrupted $\hat{\mathbf{x}}$ by simulating noise from the same distribution as the data of interest to create synthetic noisy examples. Finally, the denoiser is fine-tuned by minimizing the MSE between $\hat{\mathbf{x}}$ and the synthetic examples. If we assume additive noise, the resulting loss is of the form

$$\mathcal{L}_{\text{noise resampling}}(\mathbf{y}, \theta) = \mathbb{E}_n\left[\|(f_\theta(\hat{\mathbf{x}} + \mathbf{n}) - \hat{\mathbf{x}}\|^2\right]. \quad (7)$$

Noise resampling is reminiscent of Refs. [40, 63], which add noise to an already noisy image. When integrated in the GainTuning framework, we find the noise-resampling loss results in effective denoising in the case of additive Gaussian noise, although it generally underperforms the SURE loss.

5 Experiments and Results

We performed three different types of experiment to evaluate the performance of GainTuning **In-distribution** (test examples held out from the training set); **out-of-distribution noise** (noise level or distribution of test examples differs from training set); and **out-of-distribution signal** (test images differ in features or context from the training set). We also apply GainTuning to **real data** from a transmission electron microscope.

Our experiments make use of four **datasets**: The BSD400 natural image database [34] with test sets Set12 and Set68 [66], the Urban100 images of urban environments [22], the IUPR dataset of scanned documents [4], and a set of synthetic piecewise constant images [31] (see Section B). We demonstrate the broad applicability of GainTuning by using it in conjunction with multiple **architectures for image denoising**: DnCNN [66], BFCNN [37], UNet [50] and Blind-spot net [29] (see Section A). Finally, we compare our results to several **benchmarks**: (1) models trained on the training database, (3) CNN models adapted by fine-tuning all parameters (as opposed to just the gains), (3) a model trained only on the test data, (4) LIDIA, a specialized architecture and adaptation strategy proposed in [59]. We provide details on training and optimization in Section C.
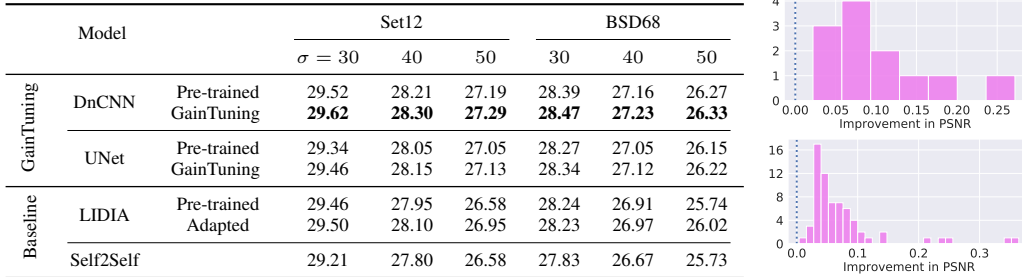
	Model		Set12			BSD68		
			$\sigma = 30$	40	50	30	40	50
GainTuning	DnCNN	Pre-trained	29.52	28.21	27.19	28.39	27.16	26.27
		GainTuning	**29.62**	**28.30**	**27.29**	**28.47**	**27.23**	**26.33**
	UNet	Pre-trained	29.34	28.05	27.05	28.27	27.05	26.15
		GainTuning	29.46	28.15	27.13	28.34	27.12	26.22
Baseline	LIDIA	Pre-trained	29.46	27.95	26.58	28.24	26.91	25.74
		Adapted	29.50	28.10	26.95	28.23	26.97	26.02
	Self2Self		29.21	27.80	26.58	27.83	26.67	25.73

Figure 3: **GainTuning achieves state-of-the-art performance.** (Left) The average PSNR on two test set of generic natural images improves after GainTuning using SURE loss function for different architectures across multiple noise levels. The CNNs are trained on generic natural images (BSD400). (Right) Histograms of improvement in PSNR achieved by DnCNN over test images from Set12 (top) and BSD68 (bottom) at $\sigma = 30$.

5.1 GainTuning surpasses state-of-the-art performance for in-distribution data

Experimental set-up. We use BSD400, a standard natural-image benchmark, corrupted with Gaussian white noise with standard deviation σ sampled uniformly from $[0, 55]$ (relative to pixel intensity range $[0, 255]$). Following [66], we evaluate performance on two independent test sets: Set12 and BSD68, corrupted with Gaussian noise with $\sigma \in \{30, 40, 50\}$.

Comparison to pre-trained CNNs. GainTuning consistently improves the performance of pre-trained CNN models. Figure 3 shows this for two different models, DnCNN [66] and UNet [50] (see also Section F.1). The SURE loss outperforms the blind-spot loss, and is slightly better than noise resampling (Table 7). The same holds for other architectures, as reported in Section F.1. On average the improvement is modest, but for some images it is quite substantial (up to 0.3 dB in PSNR for $\sigma = 30$, see histogram in Figure 3).

Comparison to other baselines. GainTuning outperforms fine-tuning based on optimizing all the parameters for different architectures and loss functions (see Section E). GainTuning clearly outperforms a Self2Self model, which is trained exclusively on the test data (Figure 3). It also outperforms the specialized architecture and adaptation process introduced in [59], with a larger gap in performance for higher noise levels.

5.2 GainTuning generalizes to new noise distributions

Experimental set-up. The same set-up as Section 5.1 is used, except that the test sets are corrupted with Gaussian noise with $\sigma \in \{70, 80\}$ (both beyond the training range of $\sigma \in [0, 55]$).

Comparison to pre-trained CNNs. Pre-trained CNN denoisers fail to generalize in this setting. GainTuning consistently improves their performance (see Figure 4).

The SURE loss again outperforms the blind-spot loss, and is slightly better than noise resampling (see Section F.2). The same holds for other architectures, as reported in Section F.2. The improvement in performance for all images is substantial (up to 12 dB in PSNR for $\sigma = 80$, see histogram in Figure 4).

Comparison to other baselines. GainTuning achieves comparable performance to a gold-standard CNN trained with supervision at all noise levels (Figure 4). GainTuning matches the performance of a bias-free CNN [37] specifically designed to generalize to out-of-distribution noise (Figure 4). GainTuning outperforms fine-tuning based on optimizing all the parameters for different architectures and loss functions (see Section E). GainTuning clearly outperforms a Self2Self model trained exclusively on the test data (Section F.2), and the LIDIA adaptation method [59].

Gaussian to Poisson generalization: Section F.2 and Figure 5 show that GainTuning can effectively adapt a CNN pre-trained for Gaussian noise removal to restore images corrupted with Poisson noise as well.
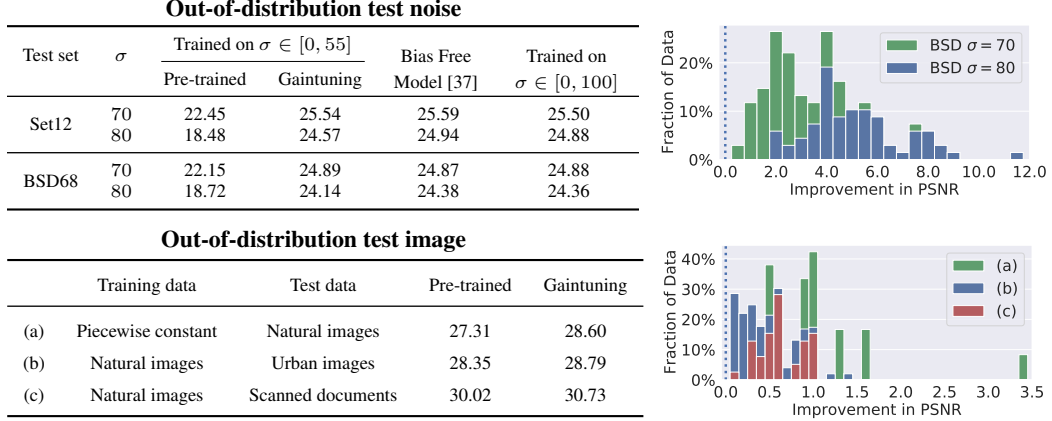
Out-of-distribution test noise

| Test set | σ | Trained on $\sigma \in [0, 55]$ | | Bias Free Model [37] | Trained on $\sigma \in [0, 100]$ |
		Pre-trained	Gaintuning		
Set12	70	22.45	25.54	25.59	25.50
	80	18.48	24.57	24.94	24.88
BSD68	70	22.15	24.89	24.87	24.88
	80	18.72	24.14	24.38	24.36

Out-of-distribution test image

	Training data	Test data	Pre-trained	Gaintuning
(a)	Piecewise constant	Natural images	27.31	28.60
(b)	Natural images	Urban images	28.35	28.79
(c)	Natural images	Scanned documents	30.02	30.73

Figure 4: **GainTuning generalizes to out-of-distribution data.** Average performance of a CNN trained to denoise at noise levels $\sigma \in [0, 55]$ improves significantly on test image with noise outside the training range, $\sigma = 70, 80$ (top) and on images with different characteristics than training data (bottom) after GainTuning. Capability of GainTuning to generalize to out-of-distribution noise is comparable to that of Bias-Free CNN [37], which is an architecture explicitly designed to generalize to noise levels outside the training range, and to that of a denoiser trained with supervision at all noise levels. (Right) Histogram showing improvement in performance for each image in the test set. The improvement is substantial across most images, reaching nearly 12dB improvement in one example. For these examples, the denoiser was DnCNN (with additive bias terms) and the GainTuning loss function was SURE. See Section F.2 for experiments with other CNN architectures and loss functions.

5.3 GainTuning generalizes to out-of-distribution image content

Experimental set-up. We evaluate the performance of GainTuning on test images that have different characteristics from the training images. We perform the following controlled experiments:

(a) Simulated piecewise constant images $\rightarrow$ **Natural images**. We pre-train CNN denoisers on simulated piecewise constant images. These images consists of constant regions (of different intensities values) with the boundaries having varied shapes such as circle and lines with different orientations (see Section B for some examples). Piecewise constant images provide a crude model for natural images [35, 44, 31]. We use GainTuning to adapt a CNN trained on this dataset to generic natural images (Set12). This experiment demonstrates the ability of GainTuning to adapt from a simple simulated dataset to a significantly more complex real dataset.

(b) Generic natural images $\rightarrow$ **Images with high self-similarity**. We apply GainTuning to adapt a CNN trained on generic natural images to images in Urban100 dataset. Urban100 consists of images of buildings and other structures typically found in an urban setting, which contain substantially more repeating/periodic structure (see Section B) than generic natural images.

(c) Generic natural images $\rightarrow$ **Images of scanned documents**. We apply GainTuning to adapt a CNN trained on generic natural images to images of scanned documents in IUPR dataset (see Section B).

All CNNs were trained for denoising Gaussian white noise with standard deviation $\sigma \in [0, 55]$ and evaluated at $\sigma = 30$.

Comparison to pre-trained CNNs. GainTuning consistently improves the performance of pre-trained CNNs in all the three experiments. Figure 4 shows this for DnCNN when GainTuning is based on SURE loss. We obtain similar results with other architectures (see Section F.3). In experiment (a), all test images show substantial improvements over the pre-trained results (average increase of roughly 1.3dB, and best case more than 3 dB, at $\sigma = 30$). We observe similar trends for experiments (b) and (c) as well, with improvements being better on an average for experiment (c). Note that we obtain similar performance increases when both *image and noise are out-of-distribution* as discussed in Section F.4.

Comparison to other baselines. In experiment (a), GainTuning outperforms methods that optimize all parameters over different architectures and loss functions (Section E). However, Self2Self trained only on test data outperforms GainTuningin this case, because the test images contain content that differs substantially from the training images. Self2Self provides the strongest form of adaptation, since it is trained exclusively on the test image, whereas the denoising properties of GainTuning are partially due to the pretraining (see Sections 7, F.3). We did not evaluate LIDIA [59] for this experiment. For experiments (b) and (c), training all parameters clearly outperforms GainTuning for case (b), but has similar performance for (c). GainTuning outperforms LIDIA on experiments (b) and (c). Self2Self trained exclusively on test data outperforms GainTuning(and LIDIA) on (b) and (c) (see Sections 7, F.3).

5.4 Application to Electron microscopy

Scientific motivation. Transmission electron microscopy (TEM) is a popular imaging technique in materials science [54, 58]. Recent advancements in TEM enable to image at high frame rates [16, 15]. These images can for example capture the dynamic, atomic-level rearrangements of catalytic systems [57, 19, 30, 32, 9], which is critical to advance our understanding of functional materials. Acquiring image series at such high temporal resolution produces data severely degraded by shot noise. Consequently, there is an acute need for denoising in this domain.

The need for adaptive denoising. Ground-truth images are not available in TEM, because measuring at high SNR is often impossible. Prior work has addressed this by using simulated training data [38, 60], whereas others have trained CNNs directly on noisy real data [52].

Dataset. We use the training set of 5583 simulated images and the test set of 40 real TEM images from [38, 60]. The data correspond to a catalytic platinum nanoparticle on a CeO_2 support (Section B).

Comparison to pre-trained CNN. A CNN [29] pre-trained on the simulated data fails to reconstruct the pattern of atoms faithfully (green box in Figure 2 (c), (e)). GainTuning applied to this CNN using the blind-spot loss correctly recovers this pattern (green box in Figure 2 (d), (e)) reconstructing the small oxygen atoms in the CeO_2 support. GainTuning with noise resampling failed to reproduce the support pattern (probably because it is absent from the initial denoised estimate) (Section F.5).

Comparison to other baselines. GainTuning clearly outperforms Self2Self, which is trained exclusively on the real data. The denoised image from Self2Self shows missing atoms and substantial artefacts (see Section F.5). We also compare GainTuning dataset to blind-spot methods using the 40 test frames [29, 52]. GainTuning clearly outperforms these methods (see Section F.5). Finally, GainTuning outperforms fine-tuning based on optimizing all the parameters, which overfits heavily (see Section E).

6 Analysis

In this section, we perform a qualitative analysis of the properties of GainTuning.

Which images benefit most from GainTuning adaptation? Section G.1 shows the images in the different test datasets for which GainTuning achieves the most and the least improvement in PSNR. The result is quite consistent over multiple architectures: the improvement in performance achieved by GainTuning is larger if the test image contains highly repetitive patterns. This makes intuitive sense; the repetitions effectively provide multiple examples from which to learn these patterns during the unsupervised refinement.

Generalization via GainTuning. Section G.2 shows that GainTuning can achieve generalization to images that are similar to the test image used for adaptation.

How does GainTuning adapt to out-of-distribution noise? Generalization to out-of-distribution noise provides a unique opportunity to understand how GainTuning modifies the denoising function. Ref. [37] shows that the first-order Taylor approximation of denoising CNNs trained on multiple noise levels tend to have a negligible constant term, and that the growth of this term is the primary culprit for the failure of these models when tested on new noise levels. GainTuning reduces the amplitude of this constant term, facilitating generalization (See Section G.3 for more details).
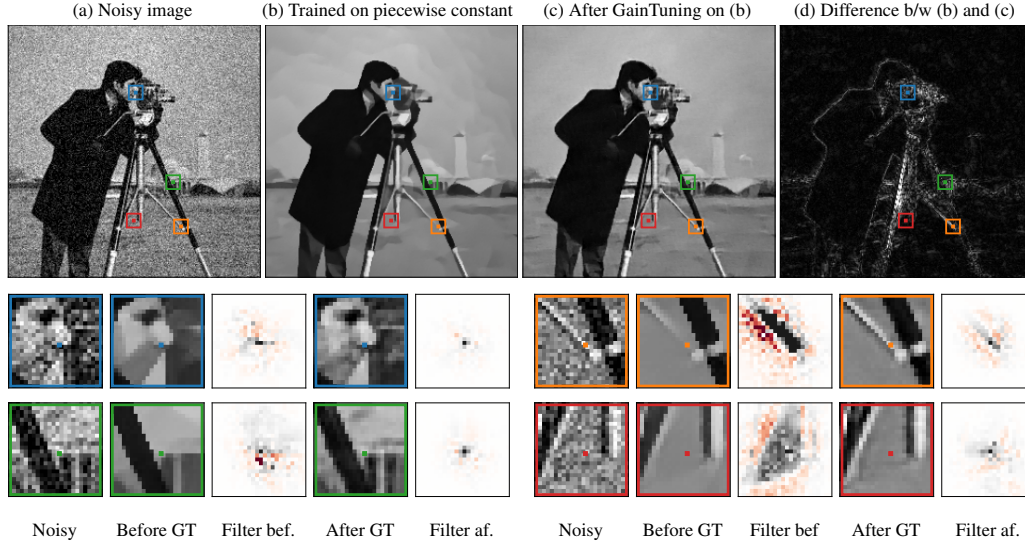
(a) Noisy image   (b) Trained on piecewise constant   (c) After GainTuning on (b)   (d) Difference b/w (b) and (c)

Noisy   Before GT   Filter bef.   After GT   Filter af.   Noisy   Before GT   Filter bef   After GT   Filter af.

Figure 5: **Adaptation to new image content**. (Top) A Bias-free CNN [37] pre-trained on piecewise constant images applied to a natural test image (a) oversmooths the image and blurs the details (b), but is able to recover more detail after applying GainTuning using SURE loss function (c). (Bottom) The CNN estimates a denoised pixel (colored pixel at the center of each image) as a linear combination of the noisy input pixels. The weighting functions (filters) of pre-trained CNN are dispersed, consistent with the training set. However, after GainTuning, the weighting functions are more precisely targeted to the local features, resulting in better recovery of details in the denoised image (c).

How does GainTuning adapt to out-of-distribution images? Figure 5 shows the result of applying a Bias-free CNN [37] trained on piecewise-constant images to natural images. Due to its learned prior, the CNN averages over large areas, ignoring fine textures. This is apparent in the equivalent linear filters obtained from a local linear approximation of the denoising function [37]. After GainTuning the model is better able to preserve the fine features, which is reflected in the equivalent filters (see Section G.4 for more details).

7   Limitations

As shown in Section 5, GainTuning improves the state of the art on benchmark datasets, adapts well to out-of-distribution noise and image content, and outperforms all existing methods on an application to real world electron-microscope data. A crucial component in the success of GainTuning is restricting the parameters that are optimized at test time. However, this constraint also limits the potential improvement in performance one can achieve, as seen when fine-tuning for test images from the Urban100 and IUPR datasets, each of which contain many images with highly repetitive structure. In these cases, we observe that fine-tuning all parameters, and even training only on the test data using Self2Self can outperform GainTuning. This raises the question of how to effectively leverage training datasets for such images.

In addition, when the pre-trained denoiser is highly optimized, and the test image is within distribution, GainTuning occasionally causes a slight degradation of performance. This is atypical (3 occurrences in 412 GainTuning experiments using DnCNN and SURE), and the decreases are quite small (maximum PSNR degradation of about 0.02dB, compared to maximum improvement of nearly 12dB; see Figure 14).

8   Conclusions

We've introduced GainTuning an adaptive denoising methodology for adaptively fine-tuning a pre-trained CNN denoiser on individual test images. The method, which is general enough to be used with any denoising CNN, improves the performance of state-of-the-art CNNs on standard

denoising benchmarks, and provides even more substantial improvements when the test data differ systematically from the training data, either in noise level, noise type, or image type. We demonstrate the potential of adaptive denoising in scientific imaging through an application to electron microscopy. Here, GainTuning is able to jointly exploit synthetic data and test-time adaptation to reconstruct meaningful structure (the atomic configuration of a nanoparticle and its support), which cannot be recovered through alternative approaches. A concrete challenge for future research is to combine the unsupervised denoising strategy of Self2Self, which relies heavily on dropout and ensembling, with pre-trained models. More generally, it is of interest to explore whether GainTuning can provide benefits for other image-processing tasks.

Finally, we would like to comment on the potential negative societal outcomes of our work. The training of CNN models on large computational clusters contributes to carbon emissions, and therefore global warming. We hope that these effects may be offset to some extent by the potential applications of these approaches to tackle challenges such as global warming. In particular, the catalytic system studied in this work is representative of catalysts used in clean energy conversion and environmental remediation [39, 65, 42].

References

[1] BALLÉ, J., LAPARRA, V., AND SIMONCELLI, E. P. Density modeling of images using a generalized normalization transformation. In *Int'l Conf on Learning Representations (ICLR)* (San Juan, Puerto Rico, May 2016). Available at http://arxiv.org/abs/1511.06281.

[2] BALLÉ, J., LAPARRA, V., AND SIMONCELLI, E. P. End-to-end optimized image compression. In *Int'l Conf on Learning Representations (ICLR)* (Toulon, France, April 2017). Available at http://arxiv.org/abs/1611.01704.

[3] BATSON, J., AND ROYER, L. Noise2self: Blind denoising by self-supervision. In *Proceedings of the 36th International Conference on Machine Learning* (2019), pp. 524–533.

[4] BUKHARI, S. S., SHAFAIT, F., AND BREUEL, T. M. The iupr dataset of camera-captured document images. In *International Workshop on Camera-Based Document Analysis and Recognition* (2011), Springer, pp. 164–171.

[5] CARANDINI, M., AND HEEGER, D. J. Normalization as a canonical neural computation. *Nature Reviews Neuroscience 13*, 1 (2012), 51–62.

[6] CHANG, S. G., YU, B., AND VETTERLI, M. Adaptive wavelet thresholding for image denoising and compression. *IEEE Trans. Image Processing 9*, 9 (2000), 1532–1546.

[7] CHEN, T., LUCIC, M., HOULSBY, N., AND GELLY, S. On self modulation for generative adversarial networks. *arXiv preprint arXiv:1810.01365* (2018).

[8] CHEN, Y., AND POCK, T. Trainable nonlinear reaction diffusion: A flexible framework for fast and effective image restoration. *IEEE transactions on pattern analysis and machine intelligence 39*, 6 (2016), 1256–1272.

[9] CROZIER, P. A., LAWRENCE, E. L., VINCENT, J. L., AND LEVIN, B. D. Dynamic restructuring during processing: approaches to higher temporal resolution. *Microscopy and Microanalysis 25*, S2 (2019), 1464–1465.

[10] DABOV, K., FOI, A., KATKOVNIK, V., AND EGIAZARIAN, K. Image denoising by sparse 3-d transform-domain collaborative filtering. *IEEE Transactions on Image Processing* (2017), 2080–2095.

[11] DE VRIES, H., STRUB, F., MARY, J., LAROCHELLE, H., PIETQUIN, O., AND COURVILLE, A. Modulating early visual processing by language. *arXiv preprint arXiv:1707.00683* (2017).

[12] DONAHUE, J., JIA, Y., VINYALS, O., HOFFMAN, J., ZHANG, N., TZENG, E., AND DARRELL, T. Decaf: A deep convolutional activation feature for generic visual recognition. In *International conference on machine learning* (2014), PMLR, pp. 647–655.

[13] DONOHO, D., AND JOHNSTONE, I. Adapting to unknown smoothness via wavelet shrinkage. *J American Stat Assoc 90*, 432 (December 1995).

[14] ELAD, M., AND AHARON, M. Image denoising via sparse and redundant representations over learned dictionaries. *IEEE Trans. on Image processing 15*, 12 (2006), 3736–3745.

[15] ERCIUS, P., JOHNSON, I., BROWN, H., PELZ, P., HSU, S.-L., DRANEY, B., FONG, E., GOLDSCHMIDT, A., JOSEPH, J., LEE, J., AND ET AL. The 4d camera – a 87 khz frame-rate detector for counted 4d-stem experiments. *Microscopy and Microanalysis* (2020), 1–3.

[16] FARUQI, A., AND MCMULLAN, G. Direct imaging detectors for electron microscopy. *Nuclear Instruments and Methods in Physics Research Section A: Accelerators, Spectrometers, Detectors and Associated Equipment 878* (2018), 180 – 190. Radiation Imaging Techniques and Applications.

[17] GHIASI, G., LEE, H., KUDLUR, M., DUMOULIN, V., AND SHLENS, J. Exploring the structure of a real-time, arbitrary neural artistic stylization network. *arXiv preprint arXiv:1705.06830* (2017).

[18] GONG, K., GUAN, J., LIU, C.-C., AND QI, J. Pet image denoising using a deep neural network through fine tuning. *IEEE Transactions on Radiation and Plasma Medical Sciences 3*, 2 (2018), 153–161.

[19] GUO, H., SAUTET, P., AND ALEXANDROVA, A. N. Reagent-triggered isomerization of fluxional cluster catalyst via dynamic coupling. *The Journal of Physical Chemistry Letters 11*, 8 (2020), 3089–3094. PMID: 32227852.

[20] HE, J., DONG, C., AND QIAO, Y. Modulating image restoration with continual levels via adaptive feature modification layers. In *Proceedings of the IEEE/CVF Conference on Computer Vision and Pattern Recognition* (2019), pp. 11056–11064.

[21] HEL-OR, Y., AND SHAKED, D. A discriminative approach for wavelet denoising. *IEEE Trans. Image Processing* (2008).

[22] HUANG, J.-B., SINGH, A., AND AHUJA, N. Single image super-resolution from transformed self-exemplars. In *Proceedings of the IEEE conference on computer vision and pattern recognition* (2015), pp. 5197–5206.

[23] IOFFE, S., AND SZEGEDY, C. Batch normalization: Accelerating deep network training by reducing internal covariate shift. *arXiv preprint arXiv:1502.03167* (2015).

[24] JARRETT, K., KAVUKCUOGLU, K., RANZATO, M., AND LECUN, Y. What is the best multi-stage architecture for object recognition? In *2009 IEEE 12th international conference on computer vision* (2009), IEEE, pp. 2146–2153.

[25] KAKU, A., MOHAN, S., PARNANDI, A., SCHAMBRA, H., AND FERNANDEZ-GRANDA, C. Be like water: Robustness to extraneous variables via adaptive feature normalization. *arXiv preprint arXiv:2002.04019* (2020).

[26] KINGMA, D. P., AND BA, J. Adam: A method for stochastic optimization. *arXiv preprint arXiv:1412.6980* (2014).

[27] KRULL, A., BUCHHOLZ, T.-O., AND JUG, F. Noise2void - learning denoising from single noisy images. In *Proceedings of the IEEE/CVF Conference on Computer Vision and Pattern Recognition* (2019), pp. 2124–2132.

[28] KRULL, A., VICAR, T., AND JUG, F. Probabilistic noise2void: Unsupervised content-aware denoising. *arXiv preprint arXiv:1906.00651* (2019).

[29] LAINE, S., KARRAS, T., LEHTINEN, J., AND AILA, T. High-quality self-supervised deep image denoising. In *Advances in Neural Information Processing Systems 32* (2019), pp. 6970–6980.

[30] LAWRENCE, E. L., LEVIN, B. D., MILLER, B. K., AND CROZIER, P. A. Approaches to exploring spatio-temporal surface dynamics in nanoparticles with in situ transmission electron microscopy. *Microscopy and Microanalysis 26*, 1 (2020), 86–94.

[31] LEE, A. B., MUMFORD, D., AND HUANG, J. Occlusion models for natural images: A statistical study of a scale-invariant dead leaves model. *International Journal of Computer Vision 41*, 1 (2001), 35–59.

[32] LEVIN, B. D., LAWRENCE, E. L., AND CROZIER, P. A. Tracking the picoscale spatial motion of atomic columns during dynamic structural change. *Ultramicroscopy 213* (2020), 112978.

[33] LUISIER, F., BLU, T., AND UNSER, M. A new sure approach to image denoising: Interscale orthonormal wavelet thresholding. *IEEE Transactions on Image Processing 16* (2007), 593–606.

[34] MARTIN, D., FOWLKES, C., TAL, D., AND MALIK, J. A database of human segmented natural images and its application to evaluating segmentation algorithms and measuring ecological statistics. In *Proc. 8th Int'l Conf. Computer Vision* (July 2001), vol. 2, pp. 416–423.

[35] MATHERON, G. Random sets and integral geometry.

[36] METZLER, C. A., MOUSAVI, A., HECKEL, R., AND BARANIUK, R. G. Unsupervised learning with stein's unbiased risk estimator. *arXiv preprint arXiv:1805.10531* (2018).

[37] MOHAN, S., KADKHODAIE, Z., SIMONCELLI, E. P., AND FERNANDEZ-GRANDA, C. Robust and interpretable blind image denoising via bias-free convolutional neural networks. In *Proceedings of the International Conference on Learning Representations* (2020).

[38] MOHAN, S., MANZORRO, R., VINCENT, J. L., TANG, B., SHETH, D. Y., SIMONCELLI, E. P., MATTESON, D. S., CROZIER, P. A., AND FERNANDEZ-GRANDA, C. Deep denoising for scientific discovery: A case study in electron microscopy. *arXiv preprint arXiv:2010.12970* (2020).

[39] MONTINI, T., MELCHIONNA, M., MONAI, M., AND FORNASIERO, P. Fundamentals and catalytic applications of ceo2-based materials. *Chemical reviews 116*, 10 (2016), 5987–6041.

[40] MORAN, N., SCHMIDT, D., ZHONG, Y., AND COADY, P. Noisier2noise: Learning to denoise from unpaired noisy data. In *Proceedings of the IEEE/CVF Conference on Computer Vision and Pattern Recognition* (2020), pp. 12064–12072.

[41] NADO, Z., PADHY, S., SCULLEY, D., D'AMOUR, A., LAKSHMINARAYANAN, B., AND SNOEK, J. Evaluating prediction-time batch normalization for robustness under covariate shift. *arXiv preprint arXiv:2006.10963* (2020).

[42] NIE, Y., LI, L., AND WEI, Z. Recent advancements in pt and pt-free catalysts for oxygen reduction reaction. *Chemical Society Reviews 44*, 8 (2015), 2168–2201.

[43] PEREZ, E., STRUB, F., DE VRIES, H., DUMOULIN, V., AND COURVILLE, A. Film: Visual reasoning with a general conditioning layer. In *Proceedings of the AAAI Conference on Artificial Intelligence* (2018), vol. 32.

[44] PITKOW, X. Exact feature probabilities in images with occlusion. *Journal of vision 10*, 14 (2010), 42–42.

[45] PORTILLA, J., STRELA, V., WAINWRIGHT, M. J., AND SIMONCELLI, E. P. Image denoising using scale mixtures of gaussians in the wavelet domain. *IEEE Trans. Image Processing 12*, 11 (2003).

[46] QUAN, Y., CHEN, M., PANG, T., AND JI, H. Self2self with dropout: Learning self-supervised denoising from single image. In *2020 IEEE/CVF Conference on Computer Vision and Pattern Recognition (CVPR)* (2020), pp. 1887–1895.

[47] RAMANI, S., BLU, T., AND UNSER, M. Monte-carlo sure: A black-box optimization of regularization parameters for general denoising algorithms. *IEEE Transactions on image processing 17*, 9 (2008), 1540–1554.

[48] RAPHAN, M., AND SIMONCELLI, E. P. Optimal denoising in redundant representations. *IEEE Trans Image Processing 17*, 8 (Aug 2008), 1342–1352.

[49] RAPHAN, M., AND SIMONCELLI, E. P. Least squares estimation without priors or supervision. *Neural Computation 23*, 2 (Feb 2011), 374–420. Published online, Nov 2010.

[50] RONNEBERGER, O., FISCHER, P., AND BROX, T. U-net: Convolutional networks for biomedical image segmentation. *Medical Image Computing and Computer-Assisted Intervention, Springer, LNCS 9351* (2015), 234–241.

[51] SCHNEIDER, S., RUSAK, E., ECK, L., BRINGMANN, O., BRENDEL, W., AND BETHGE, M. Improving robustness against common corruptions by covariate shift adaptation. *Advances in Neural Information Processing Systems 33* (2020).

[52] SHETH, D. Y., MOHAN, S., VINCENT, J. L., MANZORRO, R., CROZIER, P. A., KHAPRA, M. M., SIMONCELLI, E. P., AND FERNANDEZ-GRANDA, C. Unsupervised deep video denoising. *arXiv preprint arXiv:2011.15045* (2020).

[53] SIMONCELLI, E. P., AND ADELSON, E. H. Noise removal via Bayesian wavelet coring. In *Proc 3rd IEEE Int'l Conf on Image Proc* (Lausanne, Sep 16-19 1996), vol. I, IEEE Sig Proc Society, pp. 379–382.

[54] SMITH, D. *CHAPTER 1: Characterization of nanomaterials using transmission electron microscopy*, 37 ed. No. 37 in RSC Nanoscience and Nanotechnology. Royal Society of Chemistry, Jan. 2015, pp. 1–29.

[55] SOLTANAYEV, S., AND CHUN, S. Y. Training and refining deep learning based denoisers without ground truth data. *arXiv preprint arXiv:1803.01314* (2018).

[56] SOLTANAYEV, S., AND CHUN, S. Y. Training deep learning based denoisers without ground truth data. In *Advances in Neural Information Processing Systems* (2018), vol. 31.

[57] SUN, G., ALEXANDROVA, A. N., AND SAUTET, P. Structural rearrangements of subnanometer cu oxide clusters govern catalytic oxidation. *ACS Catalysis 10*, 9 (2020), 5309–5317.

[58] TAO, F., AND CROZIER, P. Atomic-scale observations of catalyst structures under reaction conditions and during catalysis. *Chemical Reviews 116*, 6 (Mar. 2016), 3487–3539.

[59] VAKSMAN, G., ELAD, M., AND MILANFAR, P. Lidia: Lightweight learned image denoising with instance adaptation. In *Proceedings of the IEEE/CVF Conference on Computer Vision and Pattern Recognition Workshops* (2020), pp. 524–525.

[60] VINCENT, J. L., MANZORRO, R., MOHAN, S., TANG, B., SHETH, D. Y., SIMONCELLI, E. P., MATTESON, D. S., FERNANDEZ-GRANDA, C., AND CROZIER, P. A. Developing and evaluating deep neural network-based denoising for nanoparticle tem images with ultra-low signal-to-noise.

[61] WANG, D., SHELHAMER, E., LIU, S., OLSHAUSEN, B., DARRELL, T., BERKELEY, U., AND RESEARCH, A. tent: fully test-time adaptation by entropy minimization. In *International Conference on Learning Representations* (2021), vol. 4, p. 6.

[62] XIE, Y., WANG, Z., AND JI, S. Noise2same: Optimizing a self-supervised bound for image denoising. *Advances in Neural Information Processing Systems 33* (2020).

[63] XU, J., HUANG, Y., CHENG, M.-M., LIU, L., ZHU, F., XU, Z., AND SHAO, L. Noisy-as-clean: Learning self-supervised denoising from corrupted image. *IEEE Transactions on Image Processing 29* (2020), 9316–9329.

[64] YOSINSKI, J., CLUNE, J., BENGIO, Y., AND LIPSON, H. How transferable are features in deep neural networks? *arXiv preprint arXiv:1411.1792* (2014).

[65] YU, W., POROSOFF, M. D., AND CHEN, J. G. Review of pt-based bimetallic catalysis: from model surfaces to supported catalysts. *Chemical reviews 112*, 11 (2012), 5780–5817.

[66] ZHANG, K., ZUO, W., CHEN, Y., MENG, D., AND ZHANG, L. Beyond a gaussian denoiser: Residual learning of deep cnn for image denoising. *IEEE Transactions on Image Processing* (2017), 3142–3155.

[67] ZHANG, K., ZUO, W., AND ZHANG, L. Ffdnet: Toward a fast and flexible solution for cnn-based image denoising. *IEEE Transactions on Image Processing 27*, 9 (2018), 4608–4622.

[68] ZHANG, X., LU, Y., LIU, J., AND DONG, B. Dynamically unfolding recurrent restorer: A moving endpoint control method for image restoration. *arXiv preprint arXiv:1805.07709* (2018).

Checklist

1. For all authors...

    (a) Do the main claims made in the abstract and introduction accurately reflect the paper's contributions and scope? [Yes] All claims are supported by extensive empirical experiments

    (b) Did you describe the limitations of your work? [Yes] see Section 7

    (c) Did you discuss any potential negative societal impacts of your work? [Yes] see Section 8

    (d) Have you read the ethics review guidelines and ensured that your paper conforms to them? [Yes]

2. If you are including theoretical results...

    (a) Did you state the full set of assumptions of all theoretical results? [N/A]

    (b) Did you include complete proofs of all theoretical results? [N/A]

3. If you ran experiments...

    (a) Did you include the code, data, and instructions needed to reproduce the main experimental results (either in the supplemental material or as a URL)? [Yes] We include the main code. Main data and models are public.

    (b) Did you specify all the training details (e.g., data splits, hyperparameters, how they were chosen)? [Yes] see Section A, B, C

    (c) Did you report error bars (e.g., with respect to the random seed after running experiments multiple times)? [Yes] We report histogram of improvement in the main paper, and box plot and raw data in supplementary material, instead of just summary statistics.

    (d) Did you include the total amount of compute and the type of resources used (e.g., type of GPUs, internal cluster, or cloud provider)? [Yes] see Section C

4. If you are using existing assets (e.g., code, data, models) or curating/releasing new assets...

    (a) If your work uses existing assets, did you cite the creators? [Yes]

    (b) Did you mention the license of the assets? [N/A] see Section B

    (c) Did you include any new assets either in the supplemental material or as a URL? [Yes] Code will be made available at https://github.com/sreyas-mohan/gaintuning

    (d) Did you discuss whether and how consent was obtained from people whose data you're using/curating? [N/A]

    (e) Did you discuss whether the data you are using/curating contains personally identifiable information or offensive content? [N/A]

5. If you used crowdsourcing or conducted research with human subjects...

    (a) Did you include the full text of instructions given to participants and screenshots, if applicable? [N/A]

    (b) Did you describe any potential participant risks, with links to Institutional Review Board (IRB) approvals, if applicable? [N/A]

    (c) Did you include the estimated hourly wage paid to participants and the total amount spent on participant compensation? [N/A]

A   CNN architectures

In this section we describe the denoising architectures used for our computational experiments. All architectures except BFCNN have additive (bias) terms after every convolutional layer.

A.1   DnCNN

DnCNN [66] consists of 20 convolutional layers, each consisting of 3×3 filters and 64 channels, batch normalization [23], and a ReLU nonlinearity. It has a skip connection from the initial layer to the final layer, which has no nonlinear units.

A.2   BFCNN

We use BFCNN [37] based on DnCNN architecture, i.e, we remove all sources of additive bias, including the mean parameter of the batch-normalization in every layer (note however that the scaling parameter is preserved).

A.3   UNet

Our UNet model [50] has the following layers:

1. *conv1* - Takes in input image and maps to 32 channels with 5×5 convolutional kernels.
2. *conv2* - Input: 32 channels. Output: 32 channels. 3×3 convolutional kernels.
3. *conv3* - Input: 32 channels. Output: 64 channels. 3×3 convolutional kernels with stride 2.
4. *conv4*- Input: 64 channels. Output: 64 channels. 3×3 convolutional kernels.
5. *conv5*- Input: 64 channels. Output: 64 channels. 3×3 convolutional kernels with dilation factor of 2.
6. *conv6*- Input: 64 channels. Output: 64 channels. 3×3 convolutional kernels with dilation factor of 4.
7. *conv7*- Transpose Convolution layer. Input: 64 channels. Output: 64 channels. 4×4 filters with stride 2.
8. *conv8*- Input: 96 channels. Output: 64 channels. 3×3 convolutional kernels. The input to this layer is the concatenation of the outputs of layer *conv7* and *conv2*.
9. *conv9*- Input: 32 channels. Output: 1 channels. 5×5 convolutional kernels.

The structure is the same as in [68]. This configuration of UNet assumes even width and height, so we remove one row or column from images in with odd height or width.

A.4   Blind-spot network

We use a modified version of the blind-spot network architecture introduced in Ref. [29]. We rotate the input frames by multiples of $90°$ and process them through four separate branches (with shared weights) containing asymmetric convolutional filters that are *vertically causal*. The architecture of a branch is described in Table 1. Each branch has one input channel and one output channel. Each branch is followed by a de-rotation and the output is passed to a series of three cascaded 1×1 convolutions and non-linearity for reconstruction with 4 and 96 intermediate output channels, as in [29]. The final convolutional layer is linear and has 1 output channel.

B   Datasets

We perform controlled experiments on datasets with different signal and noise structure to evaluate the broad applicability of GainTuning (see Figure 6 for a visual summary of datasets). We describe each dataset below:

Generic natural images. We use 400 images from BSD400 [34] dataset for pre-training CNNs. We evaluate on two test sets, Set12 and Set68, with 12 and 68 images, respectively [66].

Images of urban scenes. We evaluate generalization capabilities of GainTuning using a dataset of images captured in urban settings, Urban100 [22]. These images often contain repeating patterns and structures, unlike generic natural images (see Figure 6). We evaluate GainTuning on the first 50 images from this dataset.

Images of scanned documents. We use images of scanned documents from the IUPR dataset [4]. We resized the images in IUPR dataset by a factor of 6, and used the first 50 images from the dataset for evaluation.

Simulated piecewise constant images. We use a dataset of simulated piecewise constant images. These images have constant regions with boundaries consisting of various shapes such as circles and lines with different

Name	N_{out}	Function
Input	1	
enc_conv_0	48	Convolution 3×3
enc_conv_1	48	Convolution 3×3
enc_conv_2	48	Convolution 3×3
pool_1	48	MaxPool 2×2
enc_conv_3	48	Convolution 3×3
enc_conv_4	48	Convolution 3×3
enc_conv_5	48	Convolution 3×3
pool_2	48	MaxPool 2×2
enc_conv_6	96	Convolution 3×3
enc_conv_7	96	Convolution 3×3
enc_conv_8	48	Convolution 3×3
upsample_1	48	NearestUpsample 2×2
concat_1	96	Concatenate output of pool_1
dec_conv_0	96	Convolution 3×3
dec_conv_1	96	Convolution 3×3
dec_conv_2	96	Convolution 3×3
dec_conv_3	96	Convolution 3×3
upsample_2	96	NearestUpsample 2×2
concat_2	$96+k_1$	Concatenate output of Input
dec_conv_4	96	Convolution 3×3
dec_conv_5	96	Convolution 3×3
dec_conv_6	96	Convolution 3×3
dec_conv_7	1	Convolution 3×3

Table 1: **Blind-spot network**. The convolution and pooling layers are the blind-spot variants described in Ref. [29].

orientations. The constant region has an intensity value sampled from a uniform distribution between 0 and 1 (see Figure 6). These piecewise constant images provide a crude model for natural images [35, 44, 31], and a CNN pre-trained on this dataset provides a substrate for testing the ability of GainTuning to adapt to the complexity of real-world images.

Simulated transmission electron microscopy data. The TEM image data used in this work correspond to images from a widely utilized catalytic system, which consist of platinum (Pt) nanoparticles supported on a larger cerium (IV) oxide (CeO_2) nanoparticle. We use the simulated TEM image dataset introduced in Ref. [38] for pre-training CNNs. The simulated dataset contains 1024 x 1024 images, which are binned to match the approximate pixel size of the experimentally acquired real image series (described below). To equate the intensity range of the simulated images with those acquired experimentally, the intensities of the simulated images were scaled by a factor which equalized the vacuum intensity in a single simulation to the average intensity measured over a large area of the vacuum in a single 0.025 second experimental frame (i.e., 0.45 counts per pixel in the vacuum region). Furthermore, during TEM imaging multiple electron-optical and specimen parameters can give rise to complex, non-linear modulations of the image contrast. These parameters include the objective lens defocus, the specimen thickness, the orientation of the specimen, and its crystallographic shape/structure. Various combinations of these parameters may cause the contrast of atomic columns in the image to appear as black, white, or an intermediate mixture of the two. To account for this, the simulated dataset contains various instances of defocus, tilt, thickness, and shape/structure. We refer interested readers to Ref. [38] for more details.

Real transmission electron microscopy data. The real data consist of a series of images of the Pt/CeO_2 catalyst. The images were acquired in a N_2 gas atmosphere using an aberration-corrected FEI Titan transmission electron microscope (TEM), operated at 300 kV and coupled with a Gatan K2 IS direct electron detector [38]. The detector was operated in electron counting mode with a time resolution of 0.025 sec/frame and an incident electron dose rate of 5,000 $e^-/\mathring{A}^2$/s. The electromagnetic lens system of the microscope was tuned to achieve a highly coherent parallel beam configuration with minimal low-order aberrations (e.g., astigmatism, coma), and a third-order spherical aberration coefficient of approximately -13 μm. We refer interested readers to Ref. [38] for more details.

BSD400

Set12

BSD68

Urban100

IUPR

Piecewise constant images

Figure 6: **Example dataset images**. Nine images chosen at random from each dataset.

C   Details of pre-training and GainTuning

In this section, we describe the implementation details of the pre-training process and our proposed GainTuning framework.

C.1   Overview

While performing GainTuning, we introduce a scalar multiplicative parameter (gain) in every channel of the convolutional layers in the denoising CNN. We do not introduce gain parameters in the last layer of the network. We describe the general optimization process for GainTuning here, and describe any additional modifications for specific datasets in the respective subsections.

Data. We perform GainTuning on patches extracted from the noisy image. We extracted 400×400 patches for the electron microscopy dataset, and 50×50 patches for all other datasets. We do not perform any data augmentation on the extracted patches.

BatchNorm layers during GainTuning. If the denoising CNN contains batch normalization (BN) layers (only DnCNN [66] and BFCNN [37] in our experiments), we freeze their statistics while performing GainTuning. That is, we do not re-estimate the mean and standard deviation parameter for each layer from the test data. Instead, we re-use the original values estimated from pre-training dataset.

Optimization for GainTuning. We use Adam [26] optimizer. We empirically find that training for 100 steps with a starting learning rate of 10^{-4} which is reduced to 10^{-5} after the 20th step performs well across most situations (see sections below for hyper-parameters used in different experiments). Here, we define each step as a pass through 5000 random patches extracted from the test image. When performing experiments which compare optimizing all parameters to optimizing only gain during the adaptation process, we kept the learning rate constant at 10^{-5} for both options, and trained for 1000 steps.

C.2   Natural images

Pre-training dataset. Our experiments are carried out on 180×180 natural images from the Berkeley Segmentation Dataset [34]. We use a training set of 400 images. The training set is augmented via downsampling, random flips, and random rotations of patches in these images [66]. We train the CNNs on patches of size 50×50, which yields a total of 541,600 clean training patches.

Pre-training process. We train DnCNN, BFCNN and UNet using the Adam Optimizer [26] for 100 epochs with an initial learning rate of 10^{-3} and a decay factor of 0.5 for every 10 epochs after the 50th, with no early stopping [37].

GainTuning. We follow the same procedure as Section C.1.

C.3   Piecewise constant images

Pre-training dataset. We generated a synthetic dataset of piecewise constant images with the varied boundary shapes like slanted lines and circles (see Figure 6). The intensity values of the constant regions were uniformly sampled between 0 and 1. The generated patches were of size 50×50 to mimic the training process for natural images [66].

Pre-training. We train DnCNN, BFCNN and UNet using the Adam Optimizer [26] using the same process as in Section C.2. For each epoch, we generated $50,000$ random patches.

GainTuning . We follow the same procedure as Section C.1.

C.4   Electron microscope data

Pre-training dataset. Our experiments are carried out on 400×400 patches extracted from about 5000 simulated TEM introduced in Ref. [38]. The training set is augmented via downsampling, random flips, and random rotations of patches in these images [38, 60].

Optimization Details: We trained using Adam [26] optimizer with a starting learning of 10^{-4}. The learning rate was decreased by a factor of 2 at checkpoints $[20, 25, 30]$ during a total training of 40 epochs [38].

GainTuning. We performed GainTuning using Adam [26] optimizer with a constant learning rate of 10^{-5} for 100 steps. Each step consisted of 1000 randomly sampled patches of size 400×400 extracted from the test image.

C.5 Computational resources used

The computations were performed on an internal cluster equipped with NVIDIA RTX8000 and NVIDIA V100 GPUs. We used open-source pre-trained networks when available.

D Approximation for SURE

Let $\mathbf{x}$ be an N-dimensional ground-truth random vector $\mathbf{x}$ and let $\mathbf{y} := \mathbf{x} + \mathbf{n}$ be a corresponding noisy observation, where $\mathbf{n} \sim \mathcal{N}(0, \sigma_n^2 \mathbf{I})$. Stein's Unbiased Risk Estimator (SURE) provides an expression for the mean-squared error between $\mathbf{x}$ and the denoised estimate $f_\theta(\mathbf{y})$ (where f_θ denotes an arbitrary denoising function), which *only depends on the distribution of noisy observations* $\mathbf{y}$:

$$\mathbb{E}_{\mathbf{x},\mathbf{y}} \left[\frac{1}{N} \|\mathbf{x} - f_\theta(\mathbf{y})\|^2 \right] = \mathbb{E}_{\mathbf{y}} \left[\frac{1}{N} \|\mathbf{y} - f_\theta(\mathbf{y})\|^2 - \sigma^2 + \frac{2\sigma^2}{N} \sum_{k=1}^{N} \frac{\partial (f_\theta(\mathbf{y})_k)}{\partial \mathbf{y}_k} \right] \tag{8}$$

The last (divergence) term in the equation is costly to compute. Therefore, we make use of a Monte Carlo approximation of SURE introduced by Ref. [47]:

$$\sum_{k=1}^{N} \frac{\partial (f_\theta(\mathbf{y})_k)}{\partial \mathbf{y}_k} \approx \frac{1}{\epsilon N} \langle \tilde{\mathbf{n}}, f_\theta(\mathbf{y} + \epsilon \tilde{\mathbf{n}}) - f_\theta(\mathbf{y}) \rangle \tag{9}$$

where $\langle \mathbf{x}, \mathbf{y} \rangle$ represents the dot product between $\mathbf{x}$ and $\mathbf{y}$, $\tilde{n}$ represents a sample from $\mathcal{N}(0, 1)$, and ϵ represents a fixed, small, positive number. We set $\epsilon = \sigma \times 1.4 \times 10^{-4}$ for our computational experiments [55]. Equation (9) has been used in the implementation of several traditional [47], and deep learning based [36, 56, 55] denoisers.

E GainTuning prevents overfitting

We perform controlled experiments to compare test-time updating of (1) all parameters of a CNN, and (2) only the gain parameters. We briefly describe each experiment and our findings in this section.

Comparison across different cost functions. We fine-tune (a) all parameters, and (b) only gain parameters of a DnCNN [66] model when the test image is (1) in-distribution, (2) corrupted with out-of-distribution noise and (c) contains image features which are different from the training set. Fine-tuning only the gain parameters outperforms fine-tuning all parameters in all of these situations for different choices of cost functions (see Figures 7, 8 and 9)

Comparison across different architectures. We fine-tune (a) all parameters, and (b) only gain parameters of a DnCNN [66], BFCNN [37] and, UNet [50] model when the test image is (a) in-distribution, (b) corrupted with out-of-distribution noise and (c) contains image features which are different from the training set. Fine-tuning only the gain parameters often outperforms fine-tuning all parameters in all of these situations for different choices of cost functions (see Figure 10). Figure 10 shows results for a CNN trained on generic natural images and tested on images of urban scenes. In this case, training all parameters of the CNN outperforms training only the gains (see Section 7 for a discussion). Interestingly, training gains is comparable to training all parameters when we corrupt the images from urban scenes with a noise level that is also outside the training range (see Figure 11).

GainTuning does not require early stopping. Optimizing all parameters of a CNN during adaptation often results in overfitting (see Figure 10). In contrast, optimizing only the gain parameters for longer periods of time results improves performance without overfitting (Figure12).

Real electron microscopy data. We fine-tune (a) all parameters, and (b) gain parameters to adapt a CNN to real images of nanoparticle acquired through an electron microscope. The CNN was pre-trained on the simulated data described in Section B. Optimizing only the gain parameters outperforms optimizing all parameter and does not require early stopping (Figure 13)

GainTuning outperforms fine-tuning last few layers of the CNN. We compared GainTuning to selectively fine-tuning last n layers for DnCNN with $n = 20$ layers. GainTuning out-performed fine-tuning last layers by a substantial margin (see Table 2 for details). Note that gains only constitute 1.15K or 0.17% of the parameters, while fine-tuning only the last 2 layers is 37K or 5.63% parameters (about 33x more than the number of gains). The in-distribution and out-of-distribution noise consists of adapting a DnCNN trained on natural images with $\sigma \in [0, 55]$ for natural images (Set12) with $\sigma = 30$ and $\sigma = 70$ respectively. We adapted a CNN trained on piecewise constant images with $\sigma \in [0, 55]$ to natural images (Set12) with $\sigma = 30$ for out-of-distribution signal experiments.
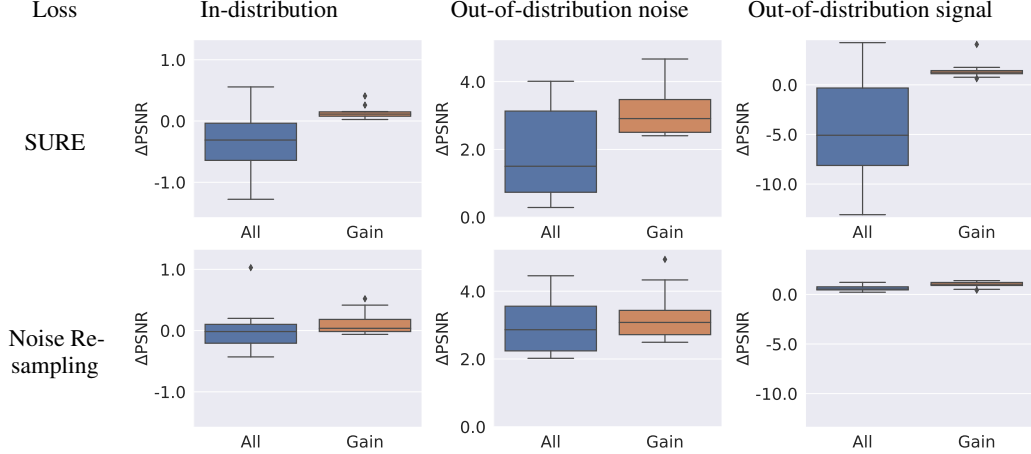
Figure 7: **GainTuning prevents overfitting.** Comparison of adaptive training of all network parameters, and GainTuning (training of gains only), using two different unsupervised objectives - SURE (top) and noise resampling (bottom). The distributions of performance improvements are shown as box plots. See Figure 8 for corresponding scatterplots. For *in-distribution*, we evaluate a CNN pre-trained on natural images corrupted with Gaussian noise of standard deviation $\sigma \in [0, 55]$ on natural images (Set12) at $\sigma = 30$. For *out-of-distribution noise* we evaluate natural images (Set12) at $\sigma = 70$. For *out-of-distribution signal* we evaluate a CNN trained on piecewise constant images at $\sigma \in [0, 55]$ on natural images (set12) at $\sigma = 30$. Please refer to Section F for details.

	All params	Fine-tuning						Only gains
		Last n layers						
		$n = 10$	$n = 4$	$n = 3$	$n = 2$	$n = 1$		
Num. params (% of total params)	668,225 (100%)	334,081 (49.95%)	111,745 (16.72%)	74,689 (11.18%)	37,633 (5.63%)	577 (0.09%)		1,152 (0.17%)
in-distribution	-0.33	0.09	0.05	0.04	0.04	0.06		**0.14**
out-of-distr. noise	1.92	1.92	2.05	2.06	2.10	2.13		**3.11**
out-of-distr. signal	-4.48	0.92	1.12	1.06	0.93	0.83		**1.45**

Table 2: **GainTuning vs selectively fine-tuning last few layers**. We compared GainTuning to selectively fine-tuning last n layers for a DnCNN with $n = 20$ layers. Table entries indicate the change in performance (i.e., the performance in PSNR after fine-tuning minus the PSNR of the pre-trained network - larger positive values are better). Across different tasks, GainTuning outperformed fine-tuning last layers by a significant margin. The in-indistribution and out-of-distribution signal consists of adapting a DnCNN trained on natural images with $\sigma \in [0, 55]$ for natural images (Set12) with $\sigma = 30$ and $\sigma = 70$ respectively. We adapted a CNN trained on piecewise constant images with $\sigma \in [0, 55]$ to natural images (Set12) with $\sigma = 30$ for out-of-distribution signal experiments.

F   Performance of GainTuning

F.1   In-distribution test image

Different architectures. We evaluated DnCNN [66], UNet [50] and BFCNN [37] architectures for this task. All models were trained on denoising Gaussian white noise of standard deviation $\sigma \in [0, 55]$ from generic natural images. Results of DnCNN and UNet are presented in Figure 3 in the main paper. Results for the BFCNN architecture are provided in Table 3.
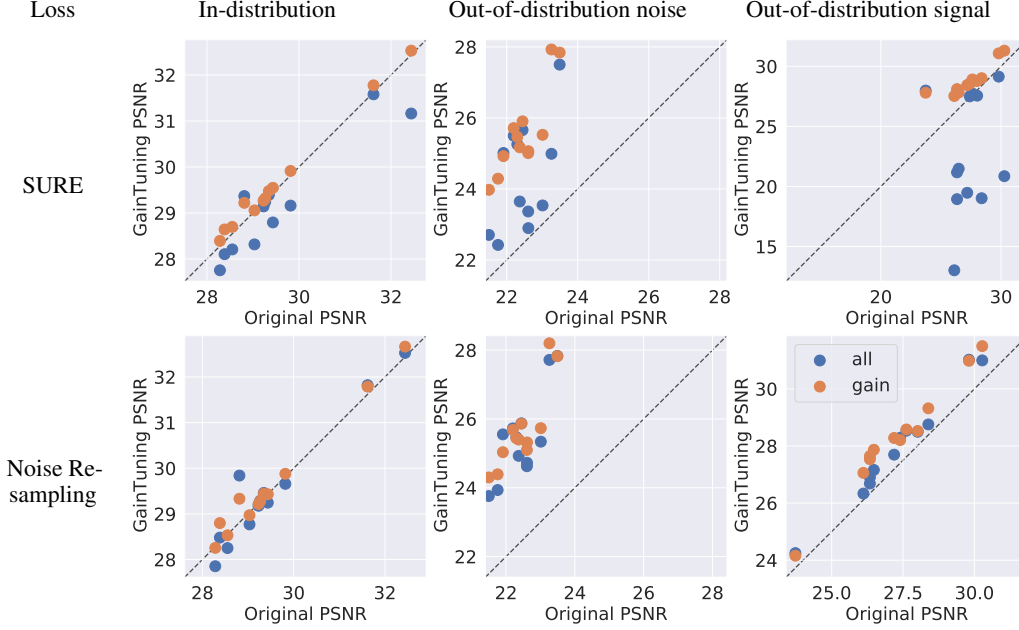
Figure 8: **GainTuning prevents overfitting.** Performance obtained from adaptively training all network parameters (blue points), compared to GainTuning (orange points) using the SURE loss, plotted against performance of the originally trained network. Each data point corresponds to one image in the dataset. The dashed line represents the identity (i.e., no improvement). Training all parameters (blue points) often leads to degraded performance, but training only the gains (orange points), leads to an improvement. For *in-distribution* test images, we evaluate a CNN pre-trained on natural images corrupted with Gaussian noise of standard deviation $\sigma \in [0, 55]$ on natural images (Set12) at $\sigma = 30$. For *out-of-distribution noise* we test on natural images (Set12) at $\sigma = 70$. For *out-of-distribution signal* we test a CNN trained on piecewise constant images at $\sigma \in [0, 55]$ on natural images (set12) at $\sigma = 30$. Please refer to Section F for details.

Model	σ	Set12		Set68	
		Pre-trained	GainTuning	Pre-trained	GainTuning
BFCNN	30	29.52	29.61	28.36	28.45

Table 3: **Results for BFCNN**. Results for BFCNN [37] architecture trained on BSD400 dataset corrupted with Gaussian noise of standard deviation $\sigma \in [0, 55]$. Results for other architectures are provided in Section 5.1.

Different cost functions. We provide the results of evaluating DnCNN architecture with different cost functions in Table 7.

Distribution of improvements. We visualize the distribution of improvements in denoising performance for different architectures after performing GainTuning using the SURE cost function in Figure 14. As discussed in Section 7, if the CNN is optimized well and the test image is in-distribution, GainTuning can degrade performance. This degradation is atypical (3 out of 408 total evaluations) and very small (maximum degradation of 0.02 dB in PSNR).

F.2 Out-of-distribution noise

Different Architectures. We summarize the results using DnCNN in Table 4 in the main paper. Figure 10 shows that the UNet architecture is also able to generalize to out-of-distribution noise.

Different Loss Functions. We provide the results of evaluating DnCNN architecture with different cost functions in Table 7.
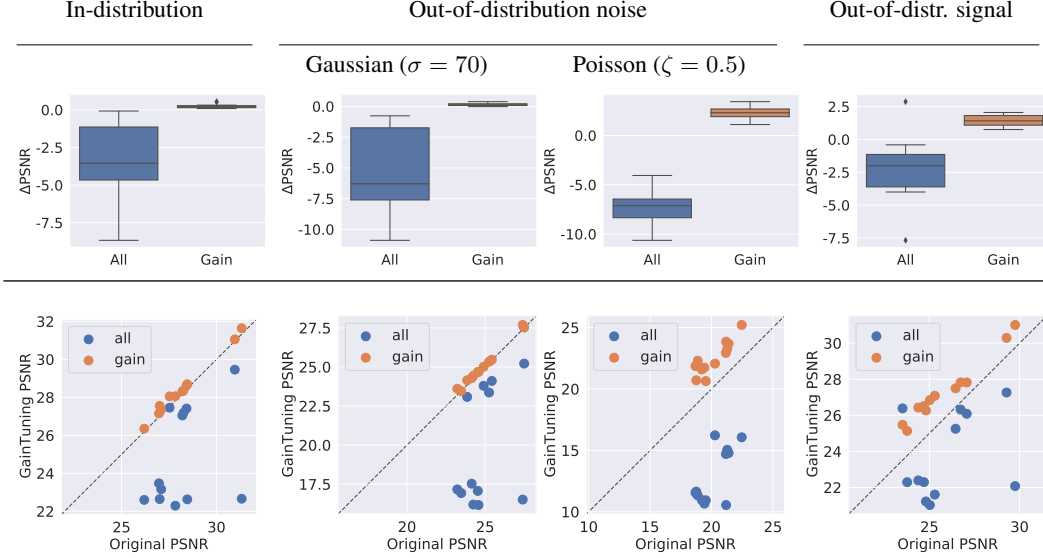
Figure 9: **GainTuning prevents overfitting.** Comparison of adaptive training of all network parameters, and GainTuning (training of gains only) using **blind-spot** cost function. The distribution of the gain in performance is visualized as a box plot. For *in-distribution*, we evaluate a CNN pre-trained on natural images corrupted with Gaussian noise of standard deviation $\sigma \in [0, 55]$ on natural images (Set12) at $\sigma = 30$. For *out-of-distribution noise* we evaluate natural images (Set12) at $\sigma = 70$ (Gaussian noise), and $\zeta = 0.5$ for Poisson noise. For *out-of-distribution signal* we evaluate a CNN trained on piecewise constant images at $\sigma \in [0, 55]$ on natural images (Set 12) at $\sigma = 30$. We used network architecture in [29] for our experiments.

| Test set | σ | Trained on $\sigma \in [0, 55]$ | | Baselines | | | | |
| | | | | Bias Free Model [37] | Trained on $\sigma \in [0, 100]$ | LIDIA [59] | | S2S [46] |
		Pre-trained	GainTuning			Pre-trained	Adapted	
Set12	70	22.45	25.54	25.59	25.50	23.69	25.01	24.61
	80	18.48	24.57	24.94	24.88	22.12	24.17	23.64
BSD68	70	22.15	24.89	24.87	24.88	23.28	24.57	24.29
	80	18.72	24.14	24.38	24.36	21.87	23.97	23.65

Table 4: **GainTuning for out-of-distribution noise**. We evaluate a DnCNN trained on generic natural images for $\sigma \in [0, 55]$ on a test set of generic natural images corrupted with $\sigma = \{70, 80\}$, which is outside the training range of the network. GainTuning is able is generalize effectively to this out-of-distribution test set. GainTuning achieves comparable performance to a network trained with supervision on a large range of noise levels ($\sigma \in [0, 100]$) an bias-free models which is an architecture explicitly designed to generalize to noise levels outside the training range. GainTuning also outperforms LIDIA [59], a specialized architecture and adaptation procedure, and Self2Self [46], a method trained exclusively on the test image.

Comparison to baselines. Table 4 summarizes the result of evaluating a DnCNN trained on generic natural images for $\sigma \in [0, 55]$ on a test set of generic natural images corrupted with $\sigma = \{70, 80\}$, which is outside the training range of the network. GainTuning is able to generalize effectively to this out-of-distribution test set. GainTuning achieves comparable performance to a network trained with supervision on a large range of noise levels ($\sigma \in [0, 100]$), and a bias-free model which is explicitly designed to generalize to noise levels outside the training range. GainTuning also outperforms LIDIA [59] (a specialized architecture and adaptation procedure). and Self2Self [46] (a method trained exclusively on the test image).
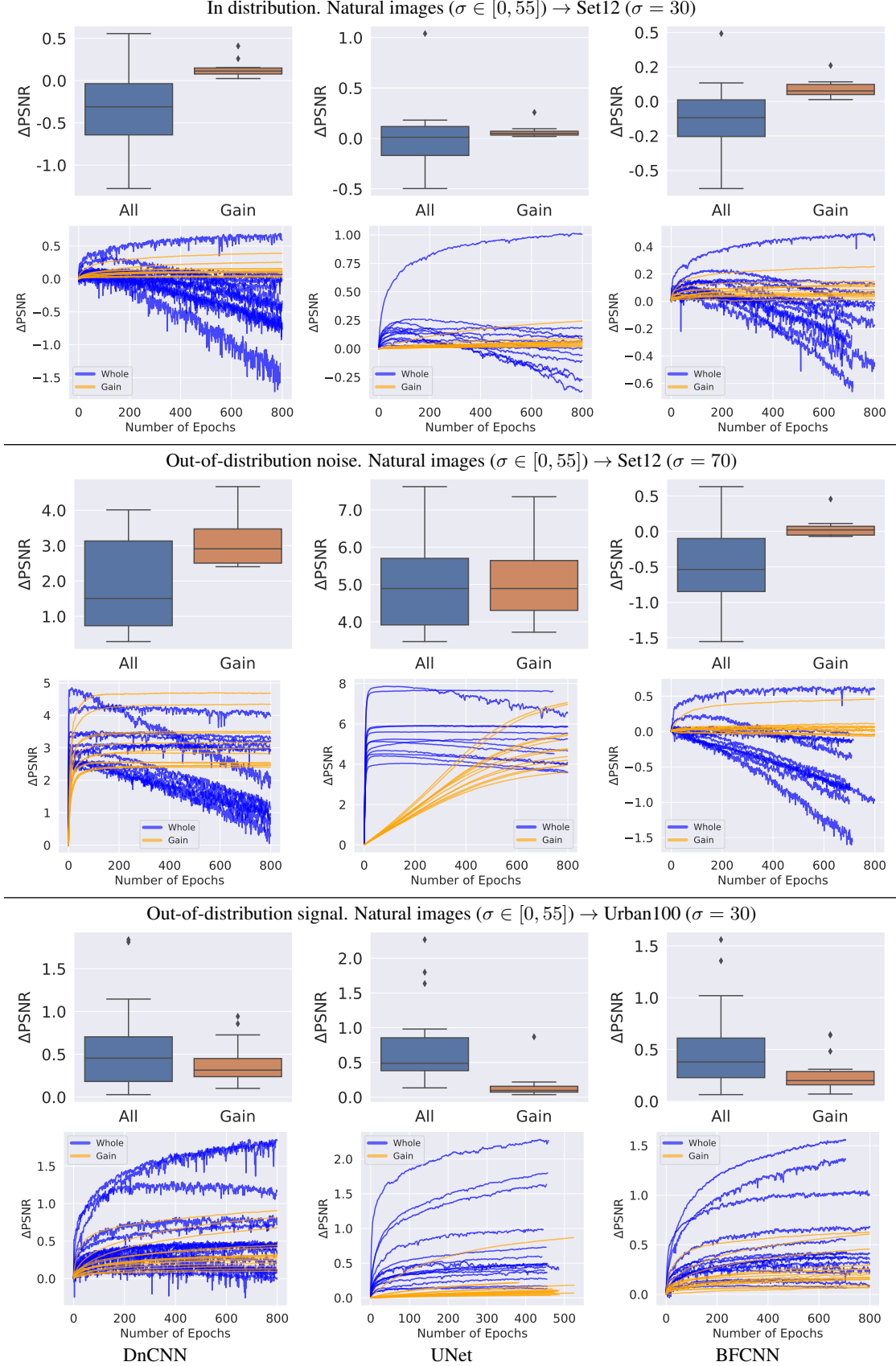
Figure 10: **GainTuning prevents overfitting**. We compare training all parameters of the network (blue) and only the gain parameters (orange) during the adaptation process. All architectures are trained using the SURE cost function.
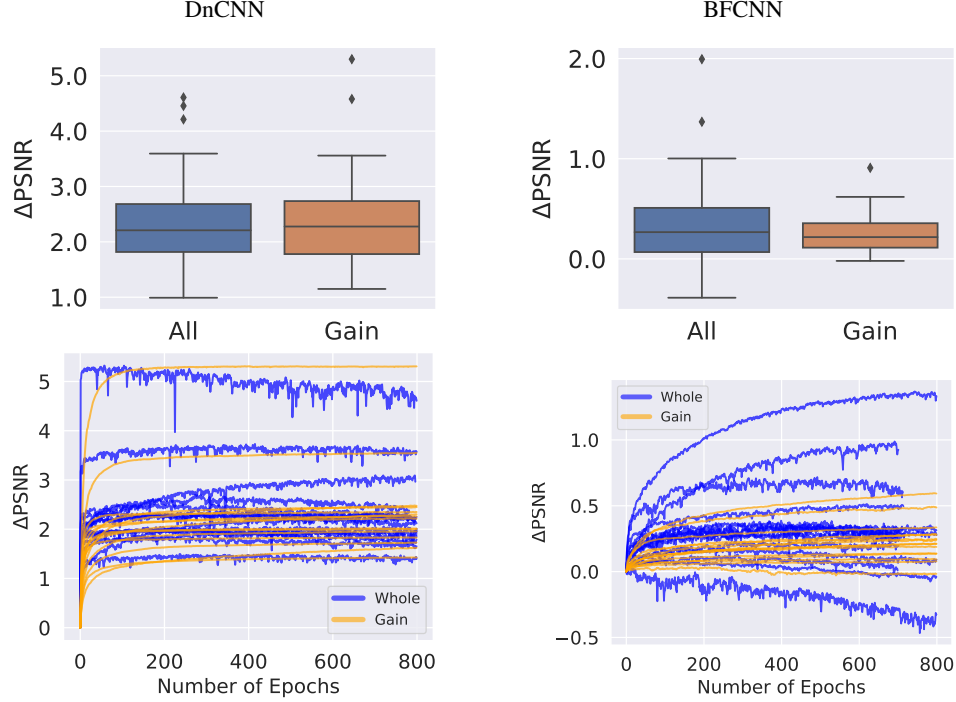
23

Figure 11: **Out-of-distribution noise and signal**. We compare training all parameters of the network (blue), and only the gain parameters (orange) during the adaptation process. The CNN is pre-trained on generic natural images corrupted with Gaussian noise of standard deviation $\sigma \in [0, 55]$. We apply GainTuning to adapt it to images of urban scenes (high self-similarity, hence different signal characteristics from natural images) corrupted with $\sigma = 70$ (which is outside the training range of noise). All architectures are trained using the SURE cost function.

F.3   Out-of-distribution image

Different Architectures. We summarize the results using DnCNN in Table 4 in the main paper. Figures 10 show that the UNet and BFCNN architectures are also able to generalize to test data with different characteristics from the training data when adapted using GainTuning .

Different Loss Functions. We provide the results of evaluating the DnCNN architecture with different cost functions in Table 7.

Comparison to baselines. Results of comparison to LIDIA [59], a specialized architecture to perform adaptation, and Self2Self [46] a method trained exclusively on the test image is summarized in Table 6. While GainTuning outperforms LIDIA, it does not match the performance of Self2Self (see Section 7 for a discussion on this).

F.4   Out-of-distribution noise and image

We evaluated the ability of GainTuning to adapt to test images which have different characteristics from those in the training set, and are additionally corrupted with a noise distribution that is different from the noise in the training set. Figure 11 shows that GainTuning is successful in this setting. The CNN was pre-trained on natural images corrupted with Gaussian white noise of standard deviation $\sigma \in [0, 55]$. We used GainTuning to adapt this CNN to a test set of images taken in urban setting (see Section B for a discussion on how it is different from natural images), corrupted with Gaussian noise of standard deviation $\sigma = 70$ (which is outside the training range of $[0, 55]$).

F.5   Application to Electron Microscopy

Comparison to pre-trained CNN. As discussed in Section 5.4, a CNN [29] pre-trained on the simulated data fails to reconstruct the pattern of atoms faithfully. We show an additional example (Figure 15) to support this. GainTuning applied to the pre-trained CNN using the blind-spot loss correctly recovers this pattern (green box in Figure 15 (d), (e)) reconstructing the small oxygen atoms in the CeO_2 support. GainTuning with noise
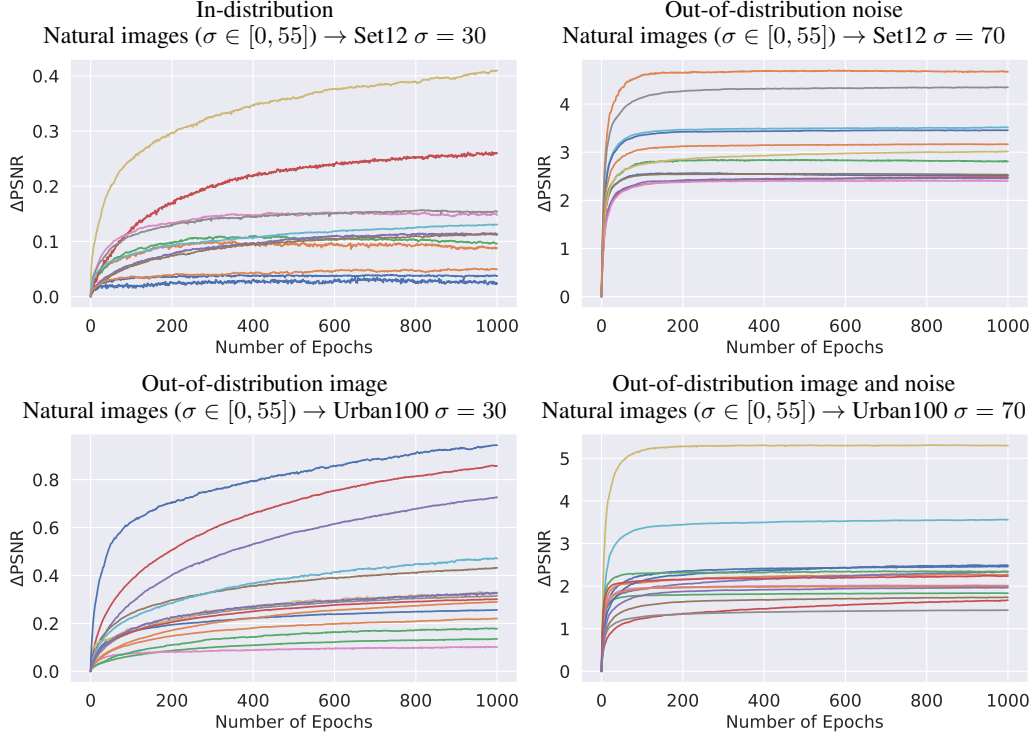
24

Figure 12: **GainTuning does not require early stopping**. We plot the improvement in performance achieved by GainTuning with the number of iterations. Each iteration step is a pass through 10000 random 50×50 patch extracted from the image. The performance achieved by optimizing only the gain parameters remains constant or monotonically increases with iteration, while training all parameters often overfits (see Figure 10)

resampling failed to reproduce the support pattern, probably because it is absent from the initial denoised estimate (see Figure 16).

Comparison to baselines. Since no ground-truth images are available for this dataset (see Section 5.4), we average 40 different acquisitions of the same underlying image to obtain an estimated reference for visual reference. We also compare GainTuning to state-of-the-art dataset based unsupervised methods, which are trained on these 40 images.

- **Blind-spot net** [29] is a CNN which is constrained to predict the intensity of a pixel as a function of the noisy pixels in its neighbourhood, without using the pixel itself. This method is competitive with the current supervised state-of-the-art CNN on photographic images. However, when applied to this dataset it produces denoised images with visible artefacts (see Figure 16). Ref. [52] shows that this may be because of the limited amount of data (40 noisy images): They trained a blind-spot net on simulated training sets of different sizes, observing that the performance on held-out data is indeed poor when the training set is small, but improves to the level of supervised approaches for large training sets.

- **Unsupervised Deep Video Denoising (UDVD)** [52] is an unsupervised method for denoising video data based on the blind-spot approach. It estimates a denoised frame using 5 consecutive noisy frames around it. Our real data consists of 40 frames acquired sequentially. UDVD produces better results than blind-spot net, but still contains visible artefacts, including missing atoms (see Figure 16). Note that UDVD uses 5 noisy images as input, and thus has more context to perform denoising than the other methods (including GainTuning).

- **Blind-spot net with early stopping**. In Ref. [52] it is shown that early stopping based on noisy held-out data can boost the performance of blind-spot nets. Here we used 35 images for training the blind-spot net and the remaining 5 images as a held-out validation set. We chose the model parameters that minimized the mean squared error between the noisy validation images and the corresponding denoised estimates. The results (shown in Figure 16) are significantly better than those of the standard
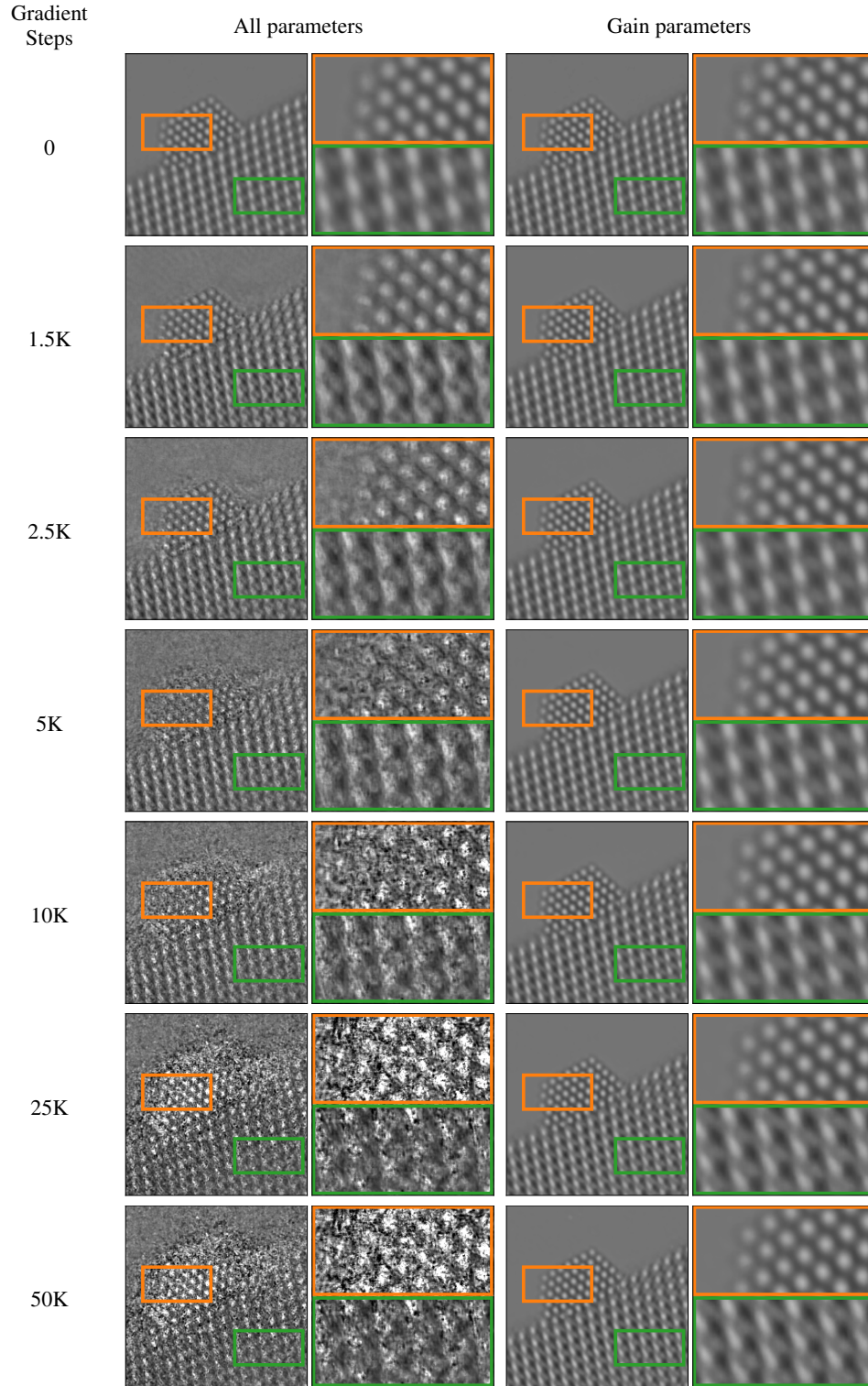
Figure 13: **GainTuning prevents overfitting in TEM data**. We compare training all parameters and only the gain parameters while adapting a CNN pre-trained on simulated TEM data to real TEM data. Training all parameters clearly overfits to the noisy image. Each gradient step is updated over two random patches of size 400×400.
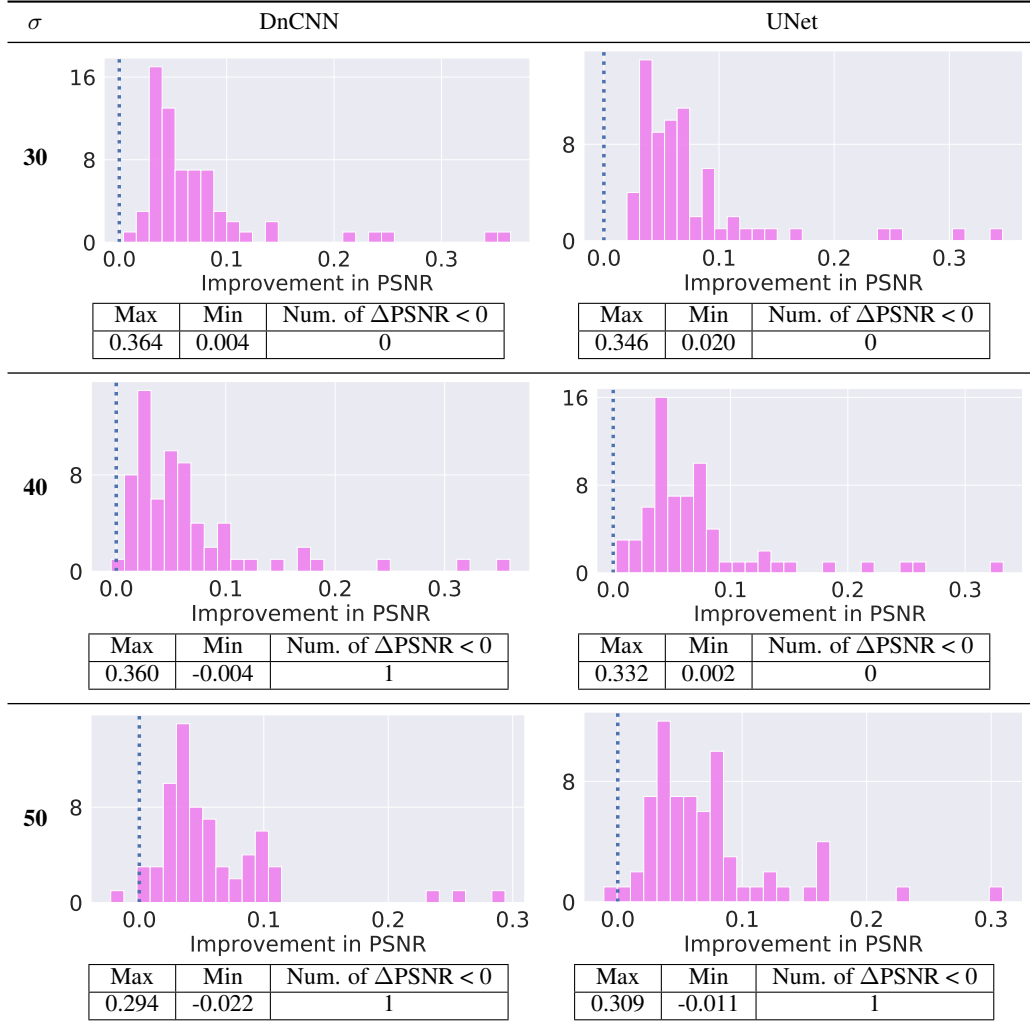
σ	DnCNN	UNet

Max	Min	Num. of ΔPSNR < 0
0.364	0.004	0

Max	Min	Num. of ΔPSNR < 0
0.346	0.020	0

Max	Min	Num. of ΔPSNR < 0
0.360	-0.004	1

Max	Min	Num. of ΔPSNR < 0
0.332	0.002	0

Max	Min	Num. of ΔPSNR < 0
0.294	-0.022	1

Max	Min	Num. of ΔPSNR < 0
0.309	-0.011	1

Figure 14: **Distribution of PSNR improvement on in-distribution test set**. Distribution of improvement on BSD68 dataset at noise levels $\sigma = \{30, 40, 50\}$ (in-distribution). When the network is well optimized, and the test image is in-distribution, GainTuning can sometimes degrade the performance of the network. This degradation is atypical (in this figure, there are only 3 occurrences of degradation out of 408 experiments), and very small (in this figure, the maximum degradation is 0.022)

(a) ζ	CNN trained on Gauss. $\sigma \in [0, 55]$		(d) Bias-free CNN trained on Gauss. $\sigma \in [0, 55]$	Improvement after GainTuning	
	(b) Pre-trained	(c) GainTuning		(e) Maximum	(f) Minimum
1	17.58	21.07	17.91	4.79	2.25
0.5	20.19	22.50	20.12	3.43	1.11
0.1	25.28	25.99	24.88	1.16	0.34

Table 5: **CNN trained on Gaussian noise generalizes to Poisson noise**. Results on applying GainTuning to a CNN pre-trained on additive Gaussian noise (which has spatially uniform variance) to test data corrupted by Poisson noise (where the variance depends on the underlying pixel values and is hence spatially variant). We evaluate on Poisson noise with three different scaling ζ values (a), where a larger value of ζ implies that the image is more noisy (if x is a clean image, the noisy image y is sampled from $\zeta \text{Pois}(x/\zeta)$ where $\text{Pois}(\lambda)$ is the PMF of Poisson distribution with parameter λ). Applying GainTuning on the CNN improves its performance (b) by a significant margin (c). GainTuning on the pre-trained CNN also outpeforms its bias-free counterpart (d), which is designed to generalize well to Gaussian noise outside the training range. The maximum improvement in PSNR (e) obtained by applying GainTuning to the pre-trained CNN (b) is substantial, and the minimum improvement in PSNR (f) is non-trivial. The CNN used here is [47] and was pre-trained on BSD400 dataset. GainTuning was performed to adapt to Set12 with Poisson noise.

	Training Data	Test Data	DnCNN [66]		Baselines		
					LIDIA [59]		S2S [46]
			Pre-trained	GainTuning	Pre-trained	Adapted	
(a)	Piecewise constant	Natural images	27.31	28.60	-	-	29.21
(b)	Natural images	Urban images	28.35	28.79	28.54	28.71	29.08
(c)	Natural images	Scanned documents	30.02	30.73	30.05	30.23	30.86

Table 6: **GainTuning for out-of-distribution images**. GainTuning generalizes robustly when the test image has different characteristics than the training data. We demonstrate this through three different experiments. (a) GainTuning provides an average of 1.3 dB in performance while adapting a CNN trained on simulated piecewise constant dataset to natural images. This controlled setting demonstrates the capability of GainTuning to adapt from a simple simulated training set to a significantly more complex real dataset. (b) GainTuning provides an average of 0.45 dB improvement in performance when a CNN trained on natural images is adapted to a dataset of images taken in urban settings. These images display a lot of repeating structure (see Section B) and hence has different characters than generic natural images. Similarly, (c) GainTuning provides an average of 0.70 dB improvement in performance when a CNN pre-trained on natural images is adapted to images of scanned documents. While GainTuning outperforms LIDIA [59], a specialized architecture designed for adapting, it does not match the performance of Self2Self (see Section 7 for a discussion on this). As noted in Section 5.3, we did not train LIDIA for (a).

blind-spot network. However, there are still noticeable artefacts, which include missing atoms. This method is similar in spirit to GainTuning - but uses a different strategy to prevent overfitting.

- **Unsupervised Deep Video Denoising (UDVD) with early stopping**. Similar to blind-spot net, performing early stopping on UDVD using 5 held-out frames greatly improves its performance [52] (Figure 16)). However, there are still noticeable artefacts in the denoised output.

F.6 Different loss functions

GainTuning can be used in conjunction with any unsupervised denoising cost function. We explore three different choices - SURE, noise resampling, and blind-spot cost functions (see Section 4), and summarize our finding in Table 7.
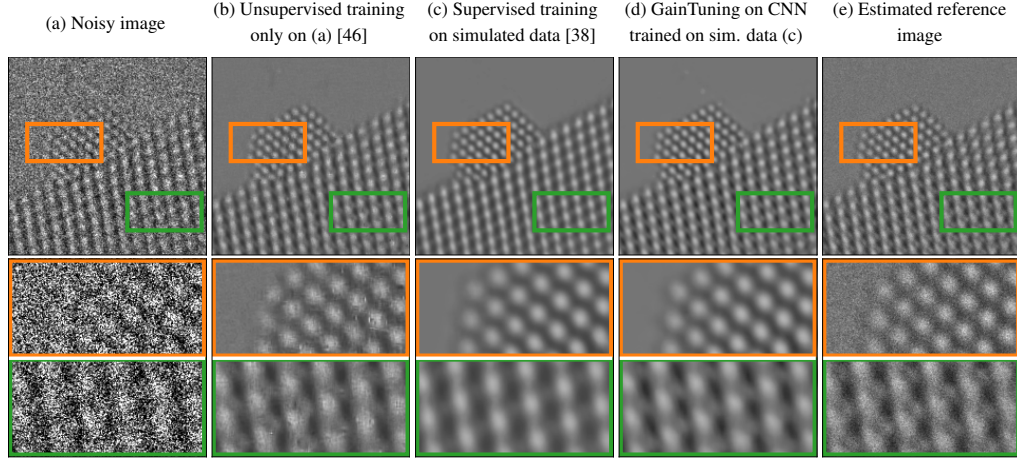
Figure 15: **Denoising results for real-world data.** (a) An experimentally-acquired atomic-resolution transmission electron microscope image of a CeO2-supported Pt nanoparticle. The image has a very low signal to noise ratio (PSNR of $\approx 3dB$). (b) Denoised image obtained using Self2Self [46], which contains significant artefacts. (c) Denoised image obtained via a CNN trained on a simulated dataset, where the pattern of the supporting atoms is not recovered faithfully (third row). (d) Denoised image obtained by adapting the CNN in (c) to the noisy test image in (a) using GainTuning. Both the nanoparticle and the support are recovered without artefacts. (e) Reference image, estimated by averaging 40 different noisy images of the same nanoparticle. See Figure 2 for an additional example.

SURE loss outperforms other choices in most experiments. Noise resampling has comparable performance to SURE when the test data is in-distribution, or when it is corrupted with out-of-distribution noise. However, noise resampling generally under-performs SURE when the test images have different features from the training images. A possible explanation for this is that noise resampling relies on the initial denoised image to fine-tune and, therefore, it may not be able to exploit features which are not present in the initial estimate. In contrast, the SURE cost function is computed on the noisy test image itself, thereby enabling it to adapt to features that the pre-trained network may be agnostic to.

Finally, adapting using blind-spot cost function often under-performs both SURE and noise resampling. The difference in performance is reduced at higher noise levels (see also Section 5.4 where we use blind-spot cost function for experiments with real TEM data with very high noise). The reason for this could be that at higher noise levels, the information contained in a single pixel becomes less relevant for computing the corresponding denoised estimate (in fact, the regularization penalty on "self pixel' for SURE cost function (Section 4) increases as the noise level increases). Therefore, the loss of performance incurred by the blind-spot cost function is diminished. At lower noise levels (particularly when the images are in-distribution), adapting using blind-spot cost function will force the pre-trained network to give up using the "self pixel", which results in a degraded performance. An alternative to adapting a generic pre-trained network using blind-spot architecture is to use a CNN that is architecturally constrained to include a blind-spot. In Table 8, we show that adapting such a CNN using blind-spot loss improves the performance its performance. However, the overall performance of this architecture is in general lower than the networks which also use the "self pixel". We refer interested readers to Ref. [29, 28, 62] for approaches to incorporate the noisy pixel into the denoised estimate.

G   Analysis

G.1   What kind of images benefit the most from adaptive denoising?

We sort images by the improvement in performance (PSNR) achieved with GainTuning. We observe that the ordering of images is similar for different models and cost functions (See Figure 17), implying that the improvement in performance is mostly dependent on the image content. The images with largest improvement typically contain repeated patterns and are more structured. Repetition of patterns effectively provides multiple samples from which the unsupervised refinement can benefit.

			GainTuning with		
		Pre-training	SURE	Noise resampling	Blind-spot (Noise2Self [3])
in distribution	Set12	29.52	29.62	**29.63**	29.50
	BSD68	28.39	**28.46**	28.40	28.36
out-of-distribution noise	Set12	18.48	**24.57**	24.11	22.93
	BSD68	18.72	**24.14**	23.65	22.50
out-of-distribution image	Piecewise constant → Natural images	27.31	**28.60**	28.29	27.39
	Natural images → Urban100	28.35	**28.79**	**28.79**	28.29
	Natural images → Scanned documents	30.02	**30.73**	30.57	29.23

Table 7: **Different loss functions for GainTuning**. Comparison of the performance of GainTuning when used in conjunction with three different loss functions. SURE loss outperforms other choices in most experiments. Noise resampling has comparable performance to SURE when the test data is in-distribution, or when it is corrupted with out-of-distribution noise. However, noise resampling generally under-performs SURE when the test images have different features from the training images. This maybe because such features are absent from the initial denoised estimate (see Section 4 for a description of the different loss functions). Finally, optimizing using blind-spot cost functions often under-performs both SURE and noise resampling, but the difference in performance is reduced as the test noise increases (see also Section 5.4 where we use blind-spot cost function for experiments with real TEM data with very high noise). This may be because, at lower noise levels, the information contained in a pixel is often crucially important to compute its denoised estimate, and blind-spot cost function ignores this information (see Section 4). Here, we implemented blind-spot cost function through masking [3], see Table 8 for results where the implemented blind-spot cost function as an architectural constraint [29].

	in-distribution		out-of-distribution image	
	Set12	BSD68	Urban100 (urban scenes)	IUPR (scanned documents)
Pre-trained	27.92	26.47	26.59	28.25
GainTuning	27.92	26.61	26.85	28.40

Table 8: **GainTuning using architecturally constrained blind-spot cost function**. We perform GainTuning using blindspot network [29] which is architecturally constrained to estimate a denoised pixel exclusively from its neighbouring pixels (excluding the pixel itself). The network was pre-trained on generic natural images corrupted with Gaussian noise of standard deviation $\sigma \in [0, 55]$. Performing GainTuning on this always increases its performance, unlike GainTuning on a generic architecture trained with supervision and adapted using blind-spot loss implemented via masking. However, note the overall performance of this architecture is in general lower than the networks which also use the "self pixel". We refer interested readers to Ref. [29, 28, 62] for approaches to incorporate the information in noisy pixel back into the denoised output, thus potentially improving the performance. Our blind-spot architecture generalizes robustly to out-of-distribution noise (since it is bias-free [37]), and therefore we do not include an out-of-distribution noise comparison in this table.
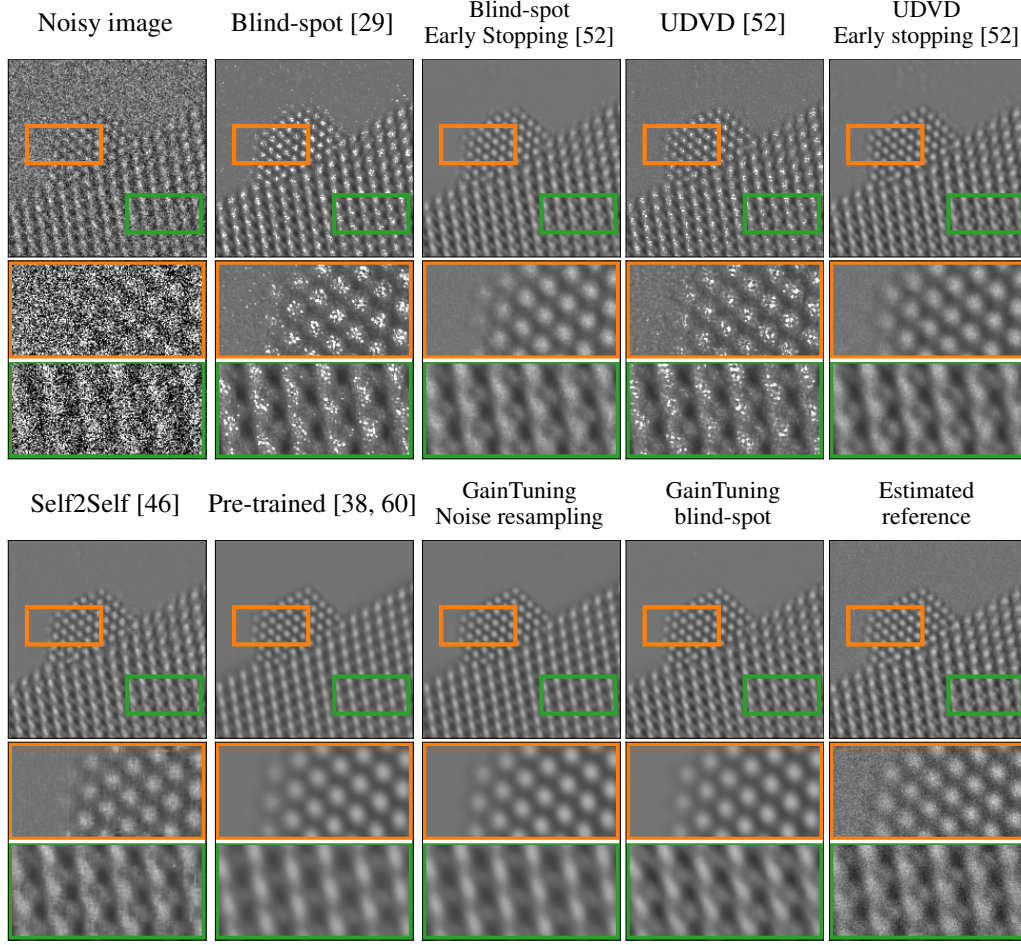
Figure 16: **Comparison with baselines for electron microscopy**. GainTuning clearly outperforms Self2Self, which is trained exclusively on the real data. The denoised image from Self2Self shows missing atoms and substantial artefacts (see Figure 15 for another example). We also compare GainTuning dataset to blind-spot methods using the 40 test frames [29, 52]. GainTuning clearly outperforms these methods.

G.2 Generalization via GainTuning

We investigate the generalization capability of GainTuning. We observe that a CNN adapted to a particular image via GainTuning generalizes effectively to other similar images. Figure 18 shows that GainTuning can achieve generalization to images that are similar to the test image used for adaptation on two examples: (1) adapting a network to an image of a scanned document generalizes to other scanned documents, and (2) adapting a a network to an image with out-of-distribution noise generalizes to other images with similar noise statistics.

G.3 How does GainTuning adapt to out-of-distribution noise?

Let $y \in \mathbb{R}^N$ be a noisy image processed by a CNN. Using the first-order Taylor approximation, the function $f : \mathbb{R}^N \to \mathbb{R}^N$ computed by a denoising CNN may be expressed as an affine function

$$f(z) = f(y) + A_y(z - y) = A_y z + b_y, \tag{10}$$

where $A_y \in \mathbb{R}^{N \times N}$ is the Jacobian of $f(\cdot)$ evaluated at input y, and $b_y \in \mathbb{R}^N$ represents the *net bias*. In [37], it was shown that the bias tends to be small for CNNs trained to denoise natural images corrupted by additive Gaussian noise, but is a primary cause of failures to generalize to noise levels not encountered during training. Figure 18 shows that GainTuning reduces the net bias of CNN, facilitating the generalization to new noise levels.
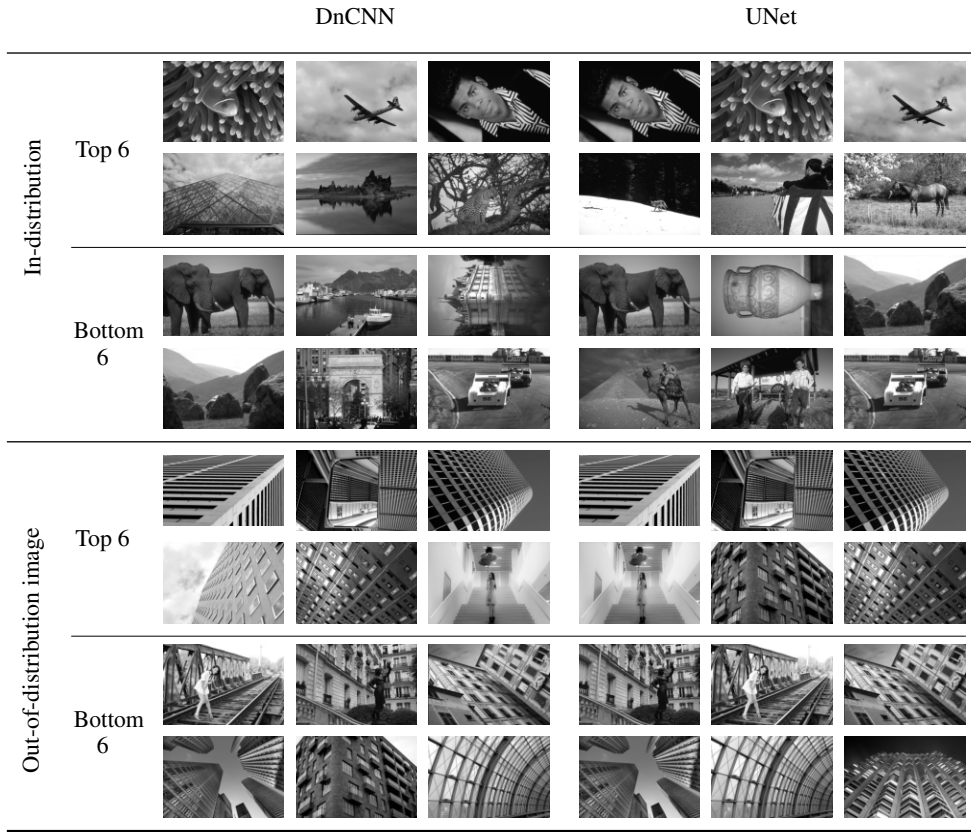
Figure 17: **What kind of images benefit the most from adaptive denoising?** We visualize the images which achieve the top 6 and bottom 6 (left top to the right bottom of each grid) improvement in performance (in PSNR) after performing GainTuning.Images with the largest improvement in performance often have highly repetitive patterns or large regions with constant intensity. Images with least improvement in performance tend to have more heterogeneous structure. Note that, in general, the distribution of improvements in performance is often skewed towards the images with minimal improvement in performance (See Figures 3, 4, and 14).

G.4   How does GainTuning adapt to out-of-distribution images?

In order to understand how GainTuning adapt to out-of-distribution images, we examine the adaptation of a CNN pre-trained on piecewise constant to natural images. Piecewise constant images have large areas with constant intensities, therefore, CNNs trained on these images tends to average over large areas. This is true even when the test image contains detailed structures. We verify this by forming the affine approximation of the network (eq. 10) and visualizing the equivalent linear filter [37], as explained below:

Let $y \in \mathbb{R}^N$ be a noisy image processed by a CNN. We process the test image using a Bias-Free CNN [37] so that the net bias b_y is zero in its first-order Taylor decomposition (10). When $b_y = 0$, (10) implies that the ith pixel of the output image is computed as an inner product between the ith row of A_y, denoted $a_y(i)$, and the input image:

$$f(y)(i) = \sum_{j=1}^{N} A_y(i,j)y(j) = a_y(i)^T y. \tag{11}$$

The vectors $a_y(i)$ can be interpreted as *adaptive filters* that produce an estimate of the denoised pixel via a weighted average of noisy pixels. As shown in Figure 5 the denoised output of CNN pre-trained on piece wise constant images is over-smoothed and the filters average over larger areas. After GainTuning the model learns to preserve the fine features much better, which is reflected in the equivalent filters.
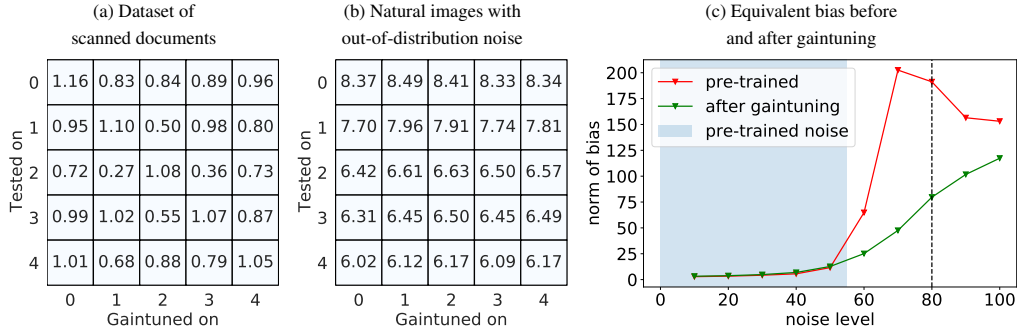
(a) Dataset of scanned documents

Tested on	0	1	2	3	4
0	1.16	0.83	0.84	0.89	0.96
1	0.95	1.10	0.50	0.98	0.80
2	0.72	0.27	1.08	0.36	0.73
3	0.99	1.02	0.55	1.07	0.87
4	1.01	0.68	0.88	0.79	1.05

Gaintuned on

(b) Natural images with out-of-distribution noise

Tested on	0	1	2	3	4
0	8.37	8.49	8.41	8.33	8.34
1	7.70	7.96	7.91	7.74	7.81
2	6.42	6.61	6.63	6.50	6.57
3	6.31	6.45	6.50	6.45	6.49
4	6.02	6.12	6.17	6.09	6.17

Gaintuned on

(c) Equivalent bias before and after gaintuning

Figure 18: **Analysis of GainTuning**. GainTuning can achieve generalization to images that are similar to the test image used for adaptation. We show this through two examples: (a) adapting a network to an image of a scanned document generalizes to other scanned documents, and (b) adapting a a network to an image with out-of-distribution noise generalizes to other images with similar noise statistics. The $(i, j)^{\text{th}}$ entry of the matrix in (a) and (b) represents the improvement in performance (measured in PNSR) when a CNN GainTuned on image j is used to denoise image i. We use 5 images with the largest improvement in performance across the dataset for (a) and (b). Finally, (c) shows that generalization to noise levels outside the training range is enabled by reducing the *equivalent bias* of the pre-trained CNN (see equation (10)).